













# VODKA-JWST: Synchronized growth of two SMBHs in a massive gas disk? A 3.8 kpc separation dual quasar at cosmic noon with JWST NIRSpec IFU

YUZO ISHIKAWA <sup>1</sup>, NADIA L. ZAKAMSKA <sup>1</sup>, YUE SHEN <sup>2</sup>, XIN LIU <sup>2,3,4</sup>, YU-CHING CHEN <sup>1,2</sup>,  
HSIANG-CHIH HWANG <sup>5</sup>, ANDREY VAYNER <sup>1,6</sup>, DAVID S. N. RUPKE <sup>7,8</sup>, SYLVAIN VEILLEUX <sup>9</sup>,  
DOMINIKA WYLEZALEK <sup>8</sup>, ARRAN C. GROSS <sup>2</sup>, SWETHA SANKAR <sup>1</sup> AND NADIA DIACHENKO<sup>1</sup>

<sup>1</sup>*Department of Physics and Astronomy, Bloomberg Center, Johns Hopkins University, Baltimore, MD 21218, USA*

<sup>2</sup>*Department of Astronomy, University of Illinois at Urbana-Champaign, Urbana, IL 61801, USA*

<sup>3</sup>*National Center for Supercomputing Applications, University of Illinois at Urbana-Champaign, Urbana, IL 61801, USA*

<sup>4</sup>*Center for Artificial Intelligence Innovation, University of Illinois at Urbana-Champaign, 1205 West Clark Street, Urbana, IL 61801, USA*

<sup>5</sup>*School of Natural Sciences, Institute for Advanced Study, 1 Einstein Drive, Princeton, NJ 08540, USA*

<sup>6</sup>*IPAC, California Institute of Technology, 1200 E. California Boulevard, Pasadena, CA 91125, USA*

<sup>7</sup>*Department of Physics, Rhodes College, 2000 N. Parkway, Memphis, TN 38112, USA*

<sup>8</sup>*Zentrum für Astronomie der Universität Heidelberg, Astronomisches Rechen-Institut, Mönchhofstr 12-14, D-69120 Heidelberg, Germany*

<sup>9</sup>*Department of Astronomy and Joint Space-Science Institute, University of Maryland, College Park, MD 20742, USA*

## ABSTRACT

The search for dual supermassive black holes (SMBHs) is of immense interest in modern astrophysics. Galaxy mergers may be an important route to fuel and to produce SMBH pairs. Actively accreting SMBH pairs can be observed as a dual quasar, which are vital probes of SMBH growth. *Gaia* observations have enabled a novel technique to systematically search for such dual quasars at previously unreachable sub-kpc scales, based on the small jitters of the light centroid as the two quasars vary stochastically. Here we present the first detailed study of a  $0.46''$ , 3.8 kpc separation, VODKA-selected dual quasar, J0749+2255, at  $z = 2.17$  using JWST/NIRSpec integral field unit spectroscopy. This is one of the most distant, small separation dual quasars identified today. Dual quasars at cosmic noon are not well characterized. We detect the faint ionized gas of the host galaxy, best traced by the narrow H $\alpha$  emission. Line ratio diagnostics show a mix of ionization from the two quasars and intense star formation. The spatially-resolved spectra of the two quasars suggest that they have very similar black hole properties (two  $M_{BH} \sim 10^9 M_{\odot}$  with large Eddington ratio reaching  $L/L_{Edd} \sim 0.2$ ) hinting at the possible synchronized growth and accretion from the same gas supply. Surprisingly, the ionized gas kinematics suggest an extended, rotating disk rather than a disturbed system that would be expected in a major gas-rich galaxy merger. While it is unclear if J0749+2255 is representative of the dual quasar evolution, the observations with JWST revealed a major puzzle. It would be interesting to see what observations of other dual quasars will show.

**Keywords:** Double quasars (406) – Supermassive black holes (1663) – Active galactic nuclei (16) – Galaxy mergers (608) – James Webb Space Telescope(2291)

## 1. INTRODUCTION

Finding and characterizing binary and dual supermassive black holes (SMBHs) is a critical frontier in understanding the formation and evolution of galaxies

and their central black holes. Galaxy mergers are often invoked as an important route to fuel and to produce SMBH pairs (Begelman et al. 1980). Following a merger of two galaxies, the two central SMBHs may inspiral into a bound binary through dynamical friction and interaction with the gas and stars (Begelman et al. 1980; Gould & Rix 2000; Milosavljević & Merritt 2001; Blaes et al. 2002; Yu 2002). To study this process, it is critical to identify SMBH pairs at different evolution-

ary stages and thus different separations: from tens of kpcs at the merger onset to  $\sim$ kpc (dual) to  $\lesssim 10$  pc (binary) when the SMBHs are gravitationally bound to each other (Colpi & Dotti 2011; Dotti et al. 2009; Volonteri et al. 2016; De Rosa et al. 2019). The rate at which black holes spiral into the center of the final galactic merger products, as well as the evolution within pc-scale separations, is very important to determine prospects of low-frequency gravitational waves (Baker et al. 2006; LIGO Scientific Collaboration & Virgo Collaboration 2016; Arzoumanian et al. 2018; EPTA Collaboration et al. 2023).

The galactic inspiraling phase is likely associated with an episode of intense accretion and winds, which play an important agent of galaxy evolution through feedback mechanisms that can heat up or expel gas that would otherwise lead to star formation (Hopkins et al. 2006). Hydrodynamical simulations predict that tidal torques are expected to cause necessary gas inflows to the central regions. When these black holes are actively accreting during inspiral, they can be observed as a dual/binary quasars. There is some evidence that major mergers may play a role in triggering the most luminous quasars, either by directly feeding gas (Barnes & Hernquist 1992; Sanders & Mirabel 1996; Di Matteo et al. 2005; Veilleux et al. 2009a,b) or by triggering an initial growth phase (McAlpine et al. 2018) until secular processes dominate SMBH growth (Hopkins & Hernquist 2009). Although the exact mechanisms of fueling remain controversial (Mechtley et al. 2016), it is clear that black hole growth requires an abundant supply of cold, dense gas that is somehow transported to the circumnuclear regions (Heckman & Best 2014).

Identifying and placing unbiased statistical constraints on the population of quasar pairs has not been possible until very recently. Past methods of candidate selection relied on mining photometric (usually optical or X-ray) quasars catalogs for spectroscopic follow-up (Comerford et al. 2015; Liu et al. 2018; Stemo et al. 2021) and are only sensitive to pairs with large angular separations  $> 1''$  corresponding to  $> 10$  kpc. Double-peaked emission lines (e.g. [O III]) may be indicative of quasar pairs (Liu et al. 2018) but may be caused by complex nuclear gas dynamics (Shen et al. 2011; Fu et al. 2012). There are only a few confirmed cases at  $\leq 1$ kpc and only one at  $\leq 10$  pc separations, many of which are serendipitously discovered objects at low redshift (Rodriguez et al. 2006; Kharb et al. 2017; Goulding et al. 2019). These discoveries lead to inhomogeneous samples that make it difficult to draw concrete comparisons between properties.

The advent of *Gaia* (Gaia Collaboration 2016) allows for a systematic search for close quasar pairs, even if unresolved by standard imaging methods. The approach of interest in this paper is Varstrometry for Off-nucleus and Dual sub-Kpc AGN (VODKA; Shen et al. 2019a; Hwang et al. 2020). Since quasars vary stochastically in the rest-frame UV and optical range (Sesar et al. 2007), asynchronous variation in flux in the unresolved components of the pair introduces an astrometric shift in the system’s photocenter observed by *Gaia* (Liu 2015, 2016). The observed *Gaia* astrometric jitters have proved to be efficient in identifying multiple point-like sources, and follow-up observations have confirmed some of these candidates as physically associated dual quasars at both low and high redshifts (Shen et al. 2019a; Hwang et al. 2020; Shen et al. 2021; Chen et al. 2022, 2023).

SDSSJ0749+2255 (J0749 henceforth) is one of the VODKA-selected dual quasars discovered by *Gaia* and confirmed through follow-up studies with the Hubble Space Telescope (HST), Gemini, Chandra, and VLA (Shen et al. 2021; Chen et al. 2023). J0749 was observed with the JWST (Gardner et al. 2006) Near-Infrared Spectrograph (NIRSpec; Jakobsen et al. 2022) instrument in the integral field unit (IFU; Böker et al. 2022) mode on UTC 2022 November 23 as part of the GO Cycle 1 program (ID: 02654; PI: Ishikawa) to uncover the faint host galaxy and characterize the gas kinematics. In this paper, we present the first spatially resolved spectroscopic observations of a  $z = 2.17$  sub-arcsec, kpc-scale separation dual quasar with *JWST*.

In Section 2 we summarize the *JWST* observations and data reduction. In Section 3 we present the spectral analyses of the dual quasars and the extended emission including point-spread-function (PSF) subtraction. We discuss quasar and host galaxy properties and implications on the dual quasar model in Section 4 and conclude in Section 5. All spectral fits are performed with wavelengths in vacuum scale. We adopt the  $\Lambda$ CDM cosmology with  $h = 0.7$ ,  $\Omega_M = 0.3$ , and  $\Omega_\Lambda = 0.7$ .

## 2. OBSERVATIONS AND DATA REDUCTION

### 2.1. Summary of J0749+2255

J0749 is an optically selected broad-line quasar at  $z = 2.17$  that was spectroscopically confirmed by the Sloan Digital Sky Survey (SDSS; Schneider et al. 2010). Although initially identified as a single quasar in SDSS, J0749 was selected as a candidate kpc-scale double quasar with *Gaia* varstrometry (Shen et al. 2021). Follow-up *HST*/F475W+F814W imaging revealed two point-like cores separated by  $\sim 0.5$  arcsec corresponding to a physical separation of  $\sim 3.8$  kpc (Shen et al. 2021; Chen et al. 2022).

Chen et al. (2023) outlined the extensive multi-wavelength imaging and spectroscopic follow-up observations of J0749. Observations in the X-ray (2 – 8 keV) with Chandra/ACIS-S and in the radio (6 and 15 GHz) with VLA A-config reveal two quasar nuclei that are spatially coincident with the HST cores – an optically brighter quasar to the southwest (J0749-SW) and a fainter quasar to the northeast (J0749-NE). Keck adaptive-optics (AO)-assisted IR/ $K_p$ -band and *HST*/F160W imaging suggests the detection of an extended host galaxy. The PSF modeling of the *HST*/F160W imaging reveals additional extended tidal tail features, possibly associated with ongoing galaxy merger interactions. Finally, spatially resolved *HST*/STIS spectroscopy and Gemini/GMOS+GNIRS spectroscopy reveal two rest-frame UV and optical quasar spectra. These spectra also showed some differences in the continuum and emission lines (Chen et al. 2023). Furthermore, imaging analyses indicated a putative nondetection of a central foreground lens galaxy. Observations of differences in the observed quasar spectra and the nondetection of a lens galaxy argued against a gravitationally lensed quasar.

In order to further test the dual quasar hypothesis and to better study its host galaxies, we use the new *JWST* NIRSpec data that covers the rest-frame optical lines. A companion paper (Chen et al. 2024) reports observations of J0749 with *JWST* MIRI IFU.

## 2.2. Observational design and data reduction

NIRSpec IFU observations were set up with two grating-filter combinations: G140M/F100LP and G235M/F170LP. This results in an effective wavelength coverage of 0.99 – 3.15  $\mu\text{m}$  and a spectral resolution of  $R \sim 400 - 1000$  across the two gratings. There were no dedicated target verification exposures. We use the NRSIRS2RAPID readout mode for improved noise performance for an effective exposure time per integration of 380 sec. and a total exposure of 3282.498 sec. We use a 9-point dither pattern to improve the spatial sampling to accurately measure and characterize the PSF. The NIRSpec/IFU field-of-view (FOV) is  $3'' \times 3''$ , which corresponds to a physical scale of roughly 25 kpc  $\times$  25 kpc.

We reduce the NIRSpec data following the methods outlined by Vayner et al. (2023a). Data reduction was completed using the STScI *JWST* pipeline<sup>1</sup> version 1.10.1 with CRDS version 11.16.2 and `mwst_1077.pmap`.

The first stage, `Detector1Pipeline`, performs standard infrared detector reductions, including dark sub-

traction, data quality flagging, bias subtraction, and cosmic ray removals, on uncalibrated files to produce rate files. We correct for  $1/f$  noise (Schlawin et al. 2020). Then, these rate files are processed by the second stage, `Spec2Pipeline`, which assigns the world coordinate system to each frame, applies flat-field corrections, flux calibrates, and extracts the 2D spectra to build a 3D cube for each dither exposure. We use the `emsm` routine instead of the `drizzle` routine to build the 3D cubes<sup>2</sup>. Vayner et al. (2023b) demonstrate that the `emsm` has a minimal detrimental effect on the PSF while improving the spectral “wiggles” that arise due to undersampling. This has been noted by other NIRSpec programs (e.g., Wylezalek et al. 2022; Veilleux et al. 2023; Vayner et al. 2023a). We also skip the imprint subtraction step due to increased noise.

After inspecting the science and “leakcal” exposure cubes, we discovered significant contamination from the Micro-Shutter Assembly (MSA). The contamination appears as a bright, “narrow line” emission scattered across the final combined NIRSpec datacube in both the spatial and spectral directions. Some of the contamination regions appear as large blobs spanning up to  $0.8''$  in diameter. Fortunately, the MSA leakage appeared at the same wavelength and spatial positions across all dither positions in both the science and “leakcal” exposures. To correct this contamination, we created an MSA-masking datacube based on the bright spaxels observed in the “leakcal” exposure and applied it to each science dither exposure. Unfortunately, this resulted in a loss of signal in the final datacube. The signal loss that results from the MSA leakage correction manifests as absorption line-like features in aperture spectra.

Finally, we combine the corrected dither datacubes into a single datacube using in-house routines (Vayner et al. 2023a; Veilleux et al. 2023). They use the Python based `reproject` method to align dither exposures and combine them into a single datacube with a spatial resolution of  $0.05''$  per spaxel. The final combined dithering pattern allows for a slightly larger FOV of roughly  $4'' \times 4''$ , which is sufficient to capture any extended emission around the two quasars. Figure 1 shows a slice of the calibrated, MSA-corrected datacube centered around  $\text{H}\alpha$ .

We perform absolute flux calibration with the *JWST*/NIRSpec commissioning standard star observation of P330E. P330E is a G2V star that was observed with the same G140M/F100LP and G235M/F170LP IFU setups (PID: 1538). We reduced the standard star

<sup>1</sup> <https://github.com/spacetelescope/jwst>

<sup>2</sup> [https://jwst-pipeline.readthedocs.io/en/latest/jwst/cube\\_build/main.html](https://jwst-pipeline.readthedocs.io/en/latest/jwst/cube_build/main.html)

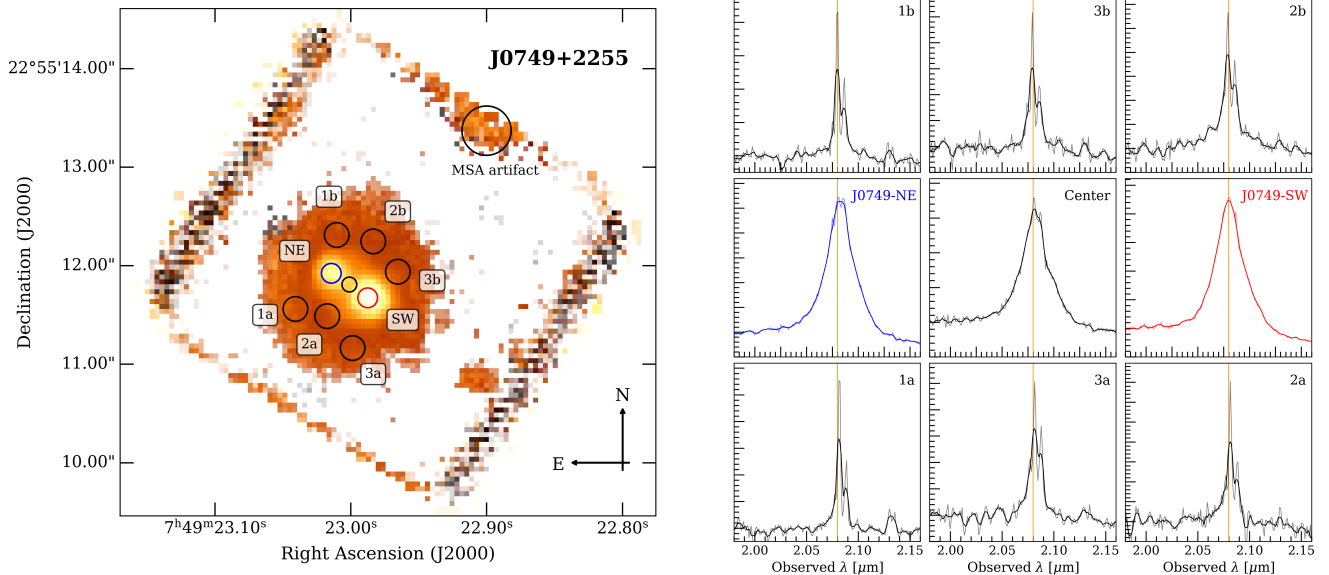


**Figure 1.** (Left) An integrated flux map of J0749 around the  $H\alpha+[N II]$  line blend is shown in the log-scale. A signal-to-noise (SNR) cut of  $SNR > 3$  to highlight the diffuse emission. Each circle overlay indicates selected aperture spectroscopy extraction that is shown in the right panel. The red and blue colors correspond to J0749-SW and J0749-NE respectively, and the black circles indicate select apertures of the host galaxy. There are significant noise artifacts along the detector edge illustrated in black blobs. (Right) Each box corresponds to the different aperture spectra of the  $H\alpha+[N II]$  line blend indicated on the left map. The fluxes are shown in the linear scale: original data in light gray lines and the boxcar smoothed spectra in thick lines. The y-axis has been normalized to highlight the line emission. We see two quasars, J0749-SW and J0749-NE, that are surrounded by extended emission traced with narrow emission lines around the same redshift but with slight velocity offsets. The vertical orange line indicates the  $H\alpha$  line centered at  $z = 2.169$ , the average redshift of the two quasars.

in the same way as the science cubes described above and flux calibrated with archival *HST*/STIS spectra from the CALSPEC database (Bohlin et al. 2014; Bohlin & Landolt 2015; Bohlin & Lockwood 2022).

### 3. SPECTRAL ANALYSIS

#### 3.1. Quasar properties

With JWST/NIRSpec IFU we confirm the detection of two quasars separated by  $0.46''$  or 3.8 kpc. First, we examine the spectra of the two quasars by taking apertures with  $r = 2$  spaxels ( $0.1''$  or  $\sim 0.8$  kpc) radii. In Figure 2 we plot the extracted JWST spectra and compare them with the previous observations from Chen et al. (2022). We find that the quasar to the southwest (J0749-SW) is about  $\times 3$  brighter than the quasar to the northeast (J0749-NE) shown in Figure 1. Both quasars exhibit a blue continuum with broad  $H\alpha$  and  $H\beta$  profiles that are indicative of Type-1 quasars.

If the two observed quasars are due to lensing by an intervening galaxy, we might expect the quasar spectra to look identical. In the case of dual quasars, we might expect the quasar spectra to be different. Interestingly, we find that the two quasars have very similar spectra. The line widths are similar, the shapes of the continua are similar, and both spectra have prominent Fe II line

complexes. However, if we take the flux ratio of the two quasars, we find that the spectra are not a one-to-one match. In particular, there are subtle differences in the Balmer line profiles, the Fe II line profiles, and the continuum redward of  $H\alpha$ . This means that J0749-NE appears slightly redder than J0749-SW.

#### 3.1.1. PyQSOFit fitting

Knowing the properties of the central SMBHs is critical to understanding the assembly history of black holes across cosmic time. We use PyQSOFit<sup>3</sup> (Guo et al. 2018; Shen et al. 2019b) to fit the 1-D spectra of the two quasars to estimate the systemic redshift and to measure the emission-line properties of each quasar. Following the treatment in Chen et al. (2023), we model each quasar spectrum as a linear combination of a pseudo-continuum (power-law, polynomial, and Fe II components), broad emission lines, and narrow emission lines. Thus, we first fit only for the pseudo-continuum with the emission lines masked out. Then we use the best continuum fit parameters as initial guesses for the global line fit and obtain the emission line properties.

<sup>3</sup> <https://github.com/legolason/PyQSOFit>

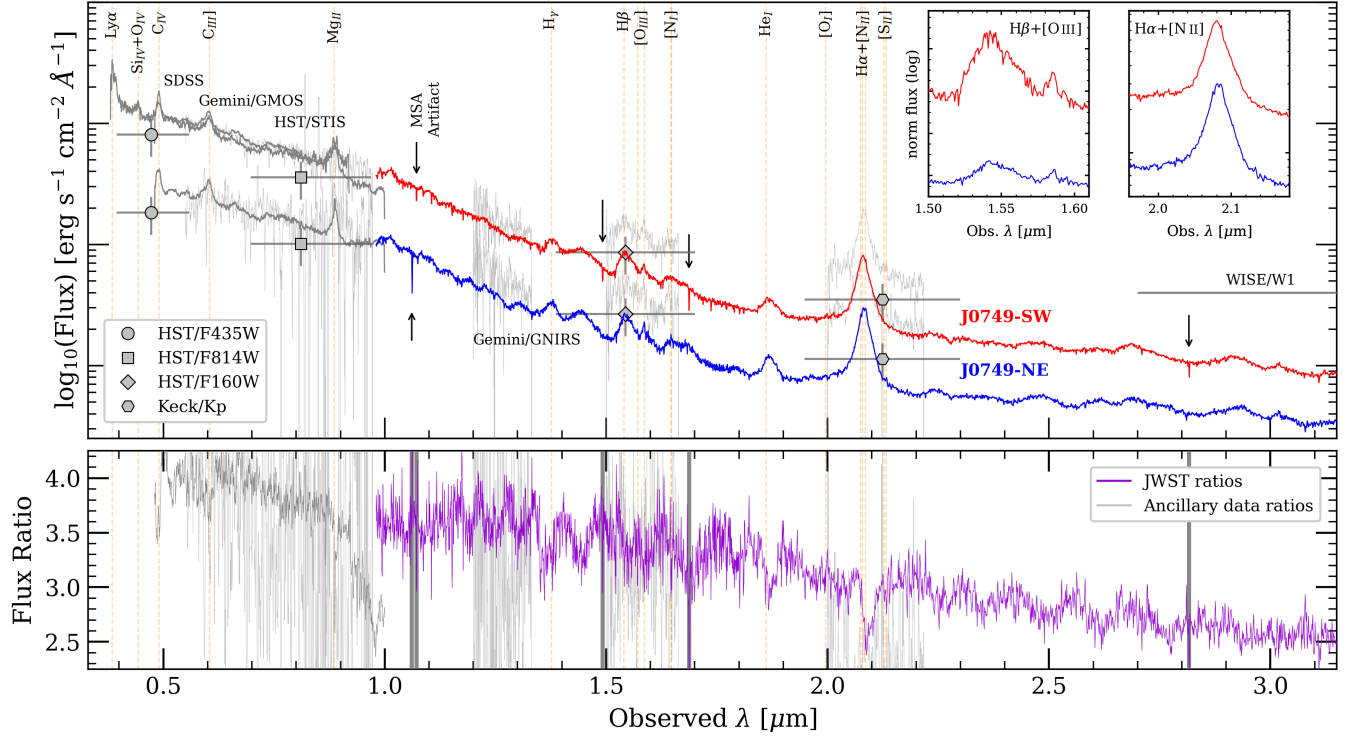


**Figure 2.** (Top) Multi-wavelength observations of the two quasars in J0749. We show data from [Chen et al. \(2023\)](#): unresolved SDSS spectroscopy in solid black line, spatially-resolved slit spectroscopy (HST/STIS, Gemini/GMOS, and Gemini/GNIRS) in faint gray lines, and spatially-resolved HST/F475W/F814W/F160W and Keck-AO/ $K_p$  photometry are indicated with gray symbols. WISE/W1 photometry is shown as a gray bar; we omit the other channels to focus on the comparison with the JWST/NIRSpec observations. The spatially resolved JWST/NIRSpec aperture spectra are shown in red (brighter J0749-SW) and blue (fainter J0749-NE). The sharp line features that resemble absorption in the JWST spectra are artifacts due to the MSA leakage correction. These spectral artifacts are indicated with black arrows. (Bottom) The flux ratio of the two quasars (J0749-SW/J0749-NE) are shown in purple, and the flux ratios corresponding to the ancillary data (HST and Gemini) are shown in light gray.

We fit for the following emission lines: Balmer lines ( $H\alpha$ ,  $H\beta$ , and  $H\gamma$ ), He  $\lambda 5877\text{\AA}$ ,  $[\text{N II}]\lambda\lambda 6549\text{\AA}, 6585\text{\AA}$ ,  $[\text{S II}]\lambda\lambda 6718\text{\AA}, 6732\text{\AA}$ , and  $[\text{O III}]\lambda\lambda 4959\text{\AA}, 5007\text{\AA}$  with a combination of broad and narrow components. We summarize the `PyQSOFit` results in Figure 3.

As hinted from the rest-frame UV spectra ([Chen et al. 2023](#)), J0749 displays strong and broad optical Fe II emission with FWHM reaching nearly  $\sim 5000 \text{ km s}^{-1}$ . In addition to the strong Fe II emission, both quasars exhibit weak  $[\text{O III}]$  emission compared to  $H\beta$ . This resulted in contamination in the  $H\beta+[\text{O III}]$  line blend, so it was unclear whether the broadest components of  $H\beta$  and  $[\text{O III}]$  were real or if they were artifacts from insufficient (or even over-subtraction) the Fe II. This somewhat complicates the attempt to establish the systemic redshift of each quasar using the peak of the  $[\text{O III}]$  narrow emission line. We obtain the following systemic redshifts:  $z = 2.1694$  for J0749-SW and  $z = 2.1686$  for J0749-NE, which is in agreement with [Chen et al. \(2023\)](#).

### 3.1.2. Quasar luminosity

From the best-fit Fe II-subtracted continuum model, we determine the optical continuum at  $\lambda = 5100\text{\AA}$ ,  $L_{5100}$ , which we use to calculate the bolometric luminosity,  $L_{bol}$ . Both J0749-NE and J0749-SW are optically luminous with  $L_{5100} \gtrsim 10^{45} \text{ erg s}^{-1}$ . Using the bolometric correction  $L_{bol} = \lambda L_{\lambda} \times \text{BC}$ , where  $\text{BC} = 10.33$  ([Richards et al. 2006](#)), we find that both quasars reach  $L_{bol} \gtrsim 10^{46} \text{ erg s}^{-1}$ . Although they show different  $L_{bol}$  by a factor of a few, it is interesting to find a quasar pair with similar emission properties. The continuum luminosity of  $L_{5100}$  could be affected by Fe II contamination of about 10-20%, comparable to photometric errors, despite `PyQSOFit` decomposition efforts.

There are subtle differences in the emission line profiles in contrast to their similar appearances in their optical continuum properties. The fit results are shown in Table 1. The FWHM of the broad component of  $H\alpha$  between J0749-SW and J0749-NE is different by nearly  $1000 \pm 200 \text{ km s}^{-1}$ . The narrow line components

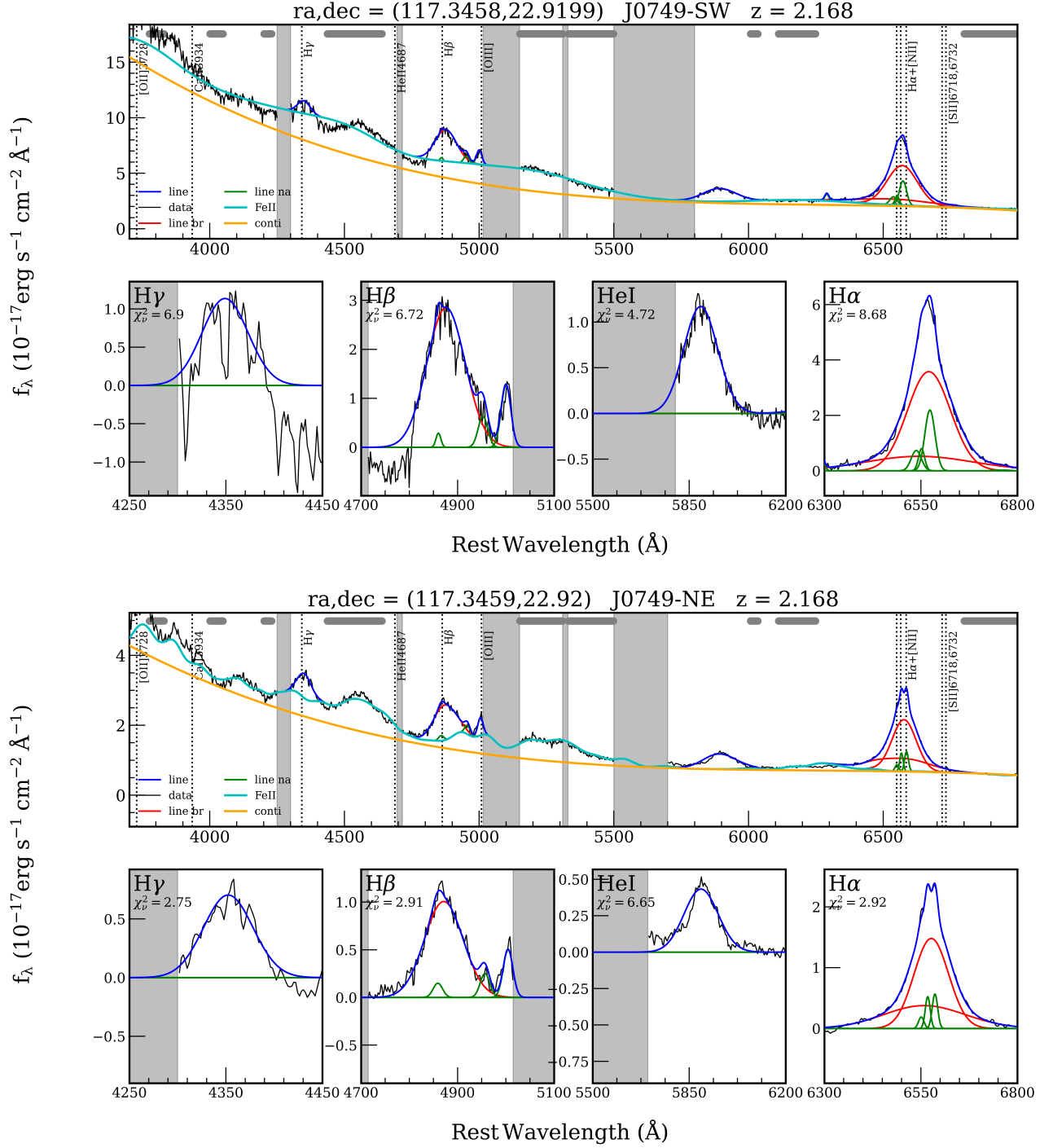


**Figure 3.** The PyQSOFit results for the brighter J0749-SW (top) and fainter J0749-NE (bottom) quasars. The shaded regions in the J0749-SW spectrum indicate the masked regions due to the MSA light leakage. The dark gray bars at the top of the plot indicate the wavelength regions used to fit the continuum and the Fe II lines.

**Table 1.** The PyQSOFit quasar line fit results of the SW (brighter) and NE (fainter) quasars. The calculated SMBH accretion properties corresponding to these fit values are shown in Table 2. The systemic redshift is calculated using the [O III] narrow line emission.

Nuclear emission-lines	Broad/Narrow	Units	J0749-SW	J0749-NE
$z_{sys}$	-	-	$2.1694 \pm 0.0001$	$2.1686 \pm 0.0001$
H $\alpha$ Flux	Broad	(erg s $^{-1}$ cm $^{-2}$ $\text{\AA}^{-1}$ )	$(650 \pm 0.3) \times 10^{-17}$	$(230 \pm 0.3) \times 10^{-17}$
H $\alpha$ Luminosity	Broad	(erg s $^{-1}$ )	$(180 \pm 0.5) \times 10^{42}$	$(640 \pm 0.5) \times 10^{42}$
H $\alpha$ FWHM	Broad	(km s $^{-1}$ )	$7500 \pm 700$	$4900 \pm 700$
H $\alpha$ Flux	Narrow	(erg s $^{-1}$ cm $^{-2}$ $\text{\AA}^{-1}$ )	$(43 \pm 0.3) \times 10^{-17}$	$(20 \pm 0.3) \times 10^{-17}$
H $\alpha$ Luminosity	Narrow	(erg s $^{-1}$ )	$(12 \pm 0.5) \times 10^{42}$	$(54 \pm 0.5) \times 10^{42}$
H $\alpha$ FWHM	Narrow	(km s $^{-1}$ )	$1400 \pm 500$	$1400 \pm 500$
H $\beta$ Flux	Broad	(erg s $^{-1}$ cm $^{-2}$ $\text{\AA}^{-1}$ )	$(290 \pm 0.3) \times 10^{-17}$	$(100 \pm 0.3) \times 10^{-17}$
H $\beta$ Luminosity	Broad	(erg s $^{-1}$ )	$(830 \pm 0.5) \times 10^{42}$	$(280 \pm 0.5) \times 10^{42}$
H $\beta$ FWHM	Broad	(km s $^{-1}$ )	$5800 \pm 700$	$5800 \pm 700$
H $\beta$ Flux	Narrow	(erg s $^{-1}$ cm $^{-2}$ $\text{\AA}^{-1}$ )	$(28 \pm 0.3) \times 10^{-17}$	$(20 \pm 0.3) \times 10^{-17}$
H $\beta$ Luminosity	Narrow	(erg s $^{-1}$ )	$(8 \pm 0.5) \times 10^{42}$	$(50 \pm 0.5) \times 10^{42}$
H $\beta$ FWHM	Narrow	(km s $^{-1}$ )	$1400 \pm 500$	$1400 \pm 500$
H $\gamma$ Flux	Broad	(erg s $^{-1}$ cm $^{-2}$ $\text{\AA}^{-1}$ )	$(100 \pm 0.3) \times 10^{-17}$	$(100 \pm 0.3) \times 10^{-17}$
H $\gamma$ Luminosity	Broad	(erg s $^{-1}$ )	$(830 \pm 0.5) \times 10^{42}$	$(280 \pm 0.5) \times 10^{42}$
He I Flux	Broad	(erg s $^{-1}$ cm $^{-2}$ $\text{\AA}^{-1}$ )	$(170 \pm 0.3) \times 10^{-17}$	$(100 \pm 0.3) \times 10^{-17}$
He I Luminosity	Broad	(erg s $^{-1}$ )	$(830 \pm 0.5) \times 10^{42}$	$(280 \pm 0.5) \times 10^{42}$
[O III] $\lambda$ 5007 $\text{\AA}$ Flux	Narrow	(erg s $^{-1}$ cm $^{-2}$ $\text{\AA}^{-1}$ )	$(32.5 \pm 0.3) \times 10^{-17}$	$(12.5 \pm 0.3) \times 10^{-17}$
[O III] $\lambda$ 5007 $\text{\AA}$ Luminosity	Narrow	(erg s $^{-1}$ )	$(11 \pm 0.5) \times 10^{42}$	$(4.4 \pm 0.5) \times 10^{42}$
[O III] $\lambda$ 5007 $\text{\AA}$ FWHM	Narrow	(km s $^{-1}$ )	$1400 \pm 500$	$1400 \pm 500$
Fe II FWHM	Broad	(km s $^{-1}$ )	$6100 \pm 700$	$3950 \pm 550$
$L_{5100}$	Broad	(erg s $^{-1}$ )	$45.90 \pm 0.001$	$45.30 \pm 0.004$
$L_{bol}$	Broad	(erg s $^{-1}$ )	$46.9 \pm 0.1$	$46.31 \pm 0.1$

**Table 2.** The SMBH accretion properties calculated based on the broad component Balmer line fits based on PyQSOFit in Table 1. The  $(a, b, c)$  coefficients for the  $M_{BH}$  calculations use the calibration by Shen & Liu (2012) and Shen et al. (2023a). We show the results for both quasars.

Method	$(a, b, c)$	Measurement	J0749-SW	J0749-NE
FWHM(H $\alpha$ ) + $L_{5100}$	(1.390, 0.555, 1.873)	$\log_{10}(M_{BH}/M_{\odot})$	$9.5 \pm 0.2$	$9.0 \pm 0.2$
		$\lambda_{Edd}$	$0.20 \pm 0.05$	$0.16 \pm 0.05$
FWHM(H $\alpha$ ) + $L_{H\alpha}$	(2.216, 0.564, 1.821)	$\log_{10}(M_{BH}/M_{\odot})$	$9.2 \pm 0.2$	$8.8 \pm 0.2$
		$\lambda_{Edd}$	$0.38 \pm 0.05$	$0.25 \pm 0.05$
FWHM(H $\beta$ ) + $L_{5100}$	(0.85, 0.5, 2.0)	$\log_{10}(M_{BH}/M_{\odot})$	$9.3 \pm 0.2$	$9.2 \pm 0.2$
		$\lambda_{Edd}$	$0.28 \pm 0.05$	$0.11 \pm 0.05$
FWHM(H $\beta$ ) + $L_{H\beta}$	(1.963, 0.401, 1.959)	$\log_{10}(M_{BH}/M_{\odot})$	$9.3 \pm 0.2$	$9.0 \pm 0.2$
		$\lambda_{Edd}$	$0.30 \pm 0.05$	$0.15 \pm 0.05$

both around  $H\beta+[O\ III]$  and  $H\alpha+[N\ II]$  are different. The emission lines associated with J0749-NE are more prominent, which produces a “pointier” spectrum compared to that of J0749-SW. Despite contamination from the Fe II emission, the equivalent widths of the [O III] emission from J0749-NE is greater than that of J0749-SW. Differences in the narrow lines are strong evidence against lensing.

### 3.1.3. SMBH properties

Using the best-fit results, we calculate the single-epoch virial black hole masses,  $M_{BH}$ , with the Shen & Liu (2012) formalism based on reverberation mapping:

$$\log_{10} \left( \frac{M_{BH}}{M_{\odot}} \right) = a + b \log_{10} \left( \frac{\lambda L_{\lambda}}{10^{44} \text{ erg s}^{-1}} \right) + c \log_{10} \left( \frac{v_{FWHM}}{\text{km s}^{-1}} \right) \quad (1)$$

We calculate  $M_{BH}$  using two different calibrations: (a)  $L_{5100}$  continuum and the broad  $H\alpha$  or  $H\beta$  line FWHM (Shen & Liu 2012; Shen et al. 2023a), and (b) the broad  $H\alpha$  or  $H\beta$  line luminosity and FWHM (Shen & Liu 2012), where  $a$ ,  $b$ , and  $c$  correspond to different calibration coefficients. Lastly, we combine the  $M_{BH}$  and  $L_{bol}$  estimates to calculate the Eddington luminosity,  $L_{Edd}$ , and the Eddington ratio,  $\lambda_{Edd} = L_{bol}/L_{Edd}$ . The calibration coefficients for the Eq.1,  $M_{BH}$ ,  $L_{Edd}$ , and  $\lambda_{Edd}$  calculations are listed in Table 2. We obtain consistent  $M_{BH}$  estimates using the different calibrations. The average  $M_{BH}$  estimates for the different methods are  $10^{9.3 \pm 0.2} M_{\odot}$  and  $10^{9.0 \pm 0.2} M_{\odot}$  for J0749-SW and J0749-NE, respectively. J0749-SW also shows a larger inferred  $\lambda_{Edd}$  of 0.29 compared to J0749-NE with 0.17. These values are roughly consistent as  $\sim 0.2$ . Although the  $M_{BH}$  estimates are in agreement with Chen et al. (2023), in this study, we obtain higher  $\lambda_{Edd}$  values likely due to improved continuum sensitivity with *JWST*. Interestingly, both quasars have similar and massive SMBH masses and Eddington ratios.

### 3.1.4. Velocity offsets

What is puzzling is that J0749 is a pair of normal Type 1 quasars with similar rest-frame UV+optical spectra (continuum and emission lines) and corresponding accretion properties ( $M_{BH}$  and  $\lambda_{Edd}$ ), despite being separated by nearly 3.8 kpc. The differences between the spectra discussed above strongly suggest that the system is a dual quasar, but even in the lensing scenario, there is always a chance that a varying nucleus produces images with slightly different spectra in an instantaneous snapshot. If the two quasars are indeed a physical pair and not lensed images, then we expect velocity offsets in the

emission lines associated with each quasar, which would be a definitive test of the dual quasar hypothesis. We investigate the presence of offsets using two methods: (a) cross-correlating the two spectra; and (b) comparing the centroids of the narrow emission lines based on the PyQSOFit results.

We cross-correlate the  $H\beta+[O\ III]$  and  $H\alpha+[N\ II]$  emission lines systems and use the flux ratios as a proxy. We fix the spectrum of J0749-SW, then offset the spectrum of J0749-NE in increments of  $\Delta v_i = 60 \text{ km s}^{-1}$ , and calculate the flux ratio for each  $\Delta v_i$ . For most offsets, we see a characteristic wavelength-varying flux profile indicating the peak of the line from one quasar corresponds to a wing of the line from the other quasar. At  $\Delta\lambda = 3.5\text{\AA}$  or  $\Delta v_i = 237 \text{ km s}^{-1}$  we find a large wavelength independent flux ratio. The expected uncertainty in velocity shifts using cross-correlation of broad Balmer lines is  $\sim 100 \text{ km s}^{-1}$  (Shen et al. 2013; Liu et al. 2014).

Similarly, we compare the centroids of the narrow [O III] emission lines. Although [O III] is fainter than the Balmer lines, we found that their centroids are more reliable. The brighter Balmer lines show complex kinematics requiring multiple broad components. We measure a centroid shift of  $\Delta\lambda \approx 3\text{\AA}$ , which corresponds to  $\Delta v \sim 180 \pm 100 \text{ km s}^{-1}$ . This is consistent with the cross-correlation results. The measured velocity offset between the two quasars is the definitive evidence that argues in favor of dual quasars rather than lensed quasars.

## 3.2. Quasar host galaxy properties

In Figure 1 we see indications of extended narrow line  $H\alpha$  emission surrounding the two quasars. The  $H\alpha$  emission is roughly at the same redshift with indications of red-/blue-shifted velocity shifts with respect to the quasars. This is a clear detection of the host galaxy(ies) of the two quasars in J0749. We describe our method of extracting the faint host galaxy emission around the quasars.

### 3.2.1. q3dfit PSF subtraction and line fitting

A major challenge to studying the faint emission around a quasar is that the quasar typically outshines its host galaxy by tens or hundreds of times. Studying the host galaxy usually involves the challenging task of carefully modeling and removing the quasar emission to extract the faint extended emission of the host galaxy. This problem is further compounded in J0749 since we have two bright quasars to account for.



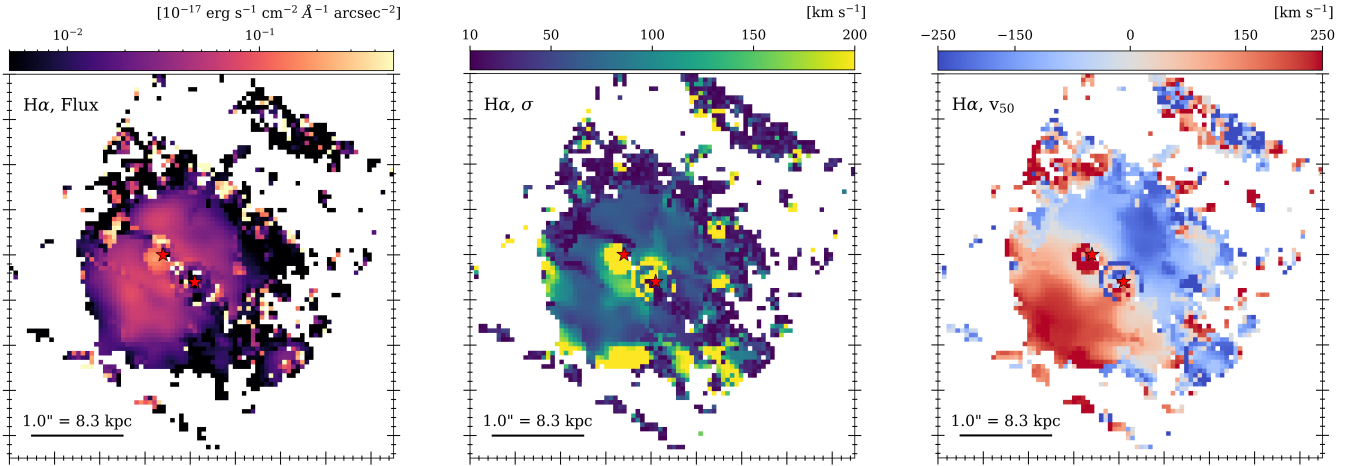


**Figure 4.** Intensity (left), velocity dispersion (center), velocity (right) maps of the quasar-subtracted, narrow-line H $\alpha$  produced with `q3dfit`. Each red star represents the subtracted quasar PSFs: J0749-NE and J0749-SW. We see that the kinematic rotation is misaligned by  $90^\circ$  with-respect-to the two quasars.

We use `q3dfit`<sup>4</sup> to model and remove the quasar PSFs to reveal the faint extended emission (Rupke et al. 2023). `q3dfit` performs maximal-contrast subtraction of the quasar PSF by using the spectral differences between the quasars and their host galaxies. `q3dfit` simultaneously fits the quasar PSF, based on an empirically determined quasar template, and the host galaxy emission model consisting of a 2-order polynomial continuum and emission lines across the NIRSPEC datacube (Vayner et al. 2023a). The quasar template is set by extracting an aperture spectrum centered on the quasar: either the brightest spaxel (default setting) or the user-defined spaxel. J0749 is a system of two quasars with two distinct spectra, so it is necessary to perform the `q3dfit` using two quasar-PSF templates. Unfortunately, `q3dfit`, out of the box, is only optimized for a galaxy system hosting one quasar. Since it is possible to set the quasar template on a user-defined spaxel, we run the quasar decomposition fits twice; one decomposition uses the quasar template centered on J0749-SW and another uses the quasar template centered on J0749-NE. Each of the quasar spectra is extracted using a circular aperture with a 2-spaxel radius ( $0.''1$ ). We make no assumptions about the shape of the host galaxy emission. Using this method, we effectively produce two sets of PSF-subtracted host galaxy datacubes corresponding to J0749-SW and J0749-NE.

We run two separate fits for each grating setting. We fit the entire cube with a single component Gaussian components for each emission line (G140M to fit H $\beta$  and [O III]; and G235M to fit H $\alpha$ , [N II], [S II], and

[O I] $\lambda$ 6300Å). The [O III] and [N II] line ratios are fixed. We assume that each Gaussian component is “kinematically tied” (Zakamska et al. 2016) across all emission lines for a given grating setting (e.g. H $\beta$  and [O III] in G140M are tied together, but not with H $\alpha$  in G235M). Successful detection of an emission line is set by two criteria:  $> 3\sigma$  peak intensity and the line widths that are greater than the instrumental width of the line-spread function. We repeat this for each quasar template.

Lastly, we combine the host galaxy fits corresponding to the two quasar templates. We iterate through each spaxel, compare the `q3dfit` line-fits for model-SW and model-NE, pick out the fits with the minimal  $\chi^2$ , and save them to the master datacube.

### 3.2.2. Host galaxy gas kinematics

We recover diffuse emission of narrow lines that are best traced by the luminous H $\alpha$  extending nearly  $2.5''$  in diameter or  $\sim 20$  kpc measured across the center of the system. In Figure 4, we show the intensity, velocity dispersion, and radial velocity maps for H $\alpha$ . For the first time, we detect the faint diffuse emission and measure its kinematics surrounding a close-separation dual quasar at  $z \sim 2$ . We see maximal radial velocity difference of  $\Delta v \sim 1000$  km s $^{-1}$  along the line perpendicular to the quasar alignment (northwest vs. southeast regions) with a blue-shifted component to the northwest and a redshifted component to the southeast. Selected aperture spectra of H $\alpha$  are shown in Figure 1. The inferred H $\alpha$  intensity and velocity maps suggest that J0749 may be hosted by a large rotating gas disk with no obvious signs of kinematic disturbance often seen in major mergers. The quasars lie in the line of nodes of the galactic

<sup>4</sup> <https://q3dfit.readthedocs.io/en/latest/index.html>

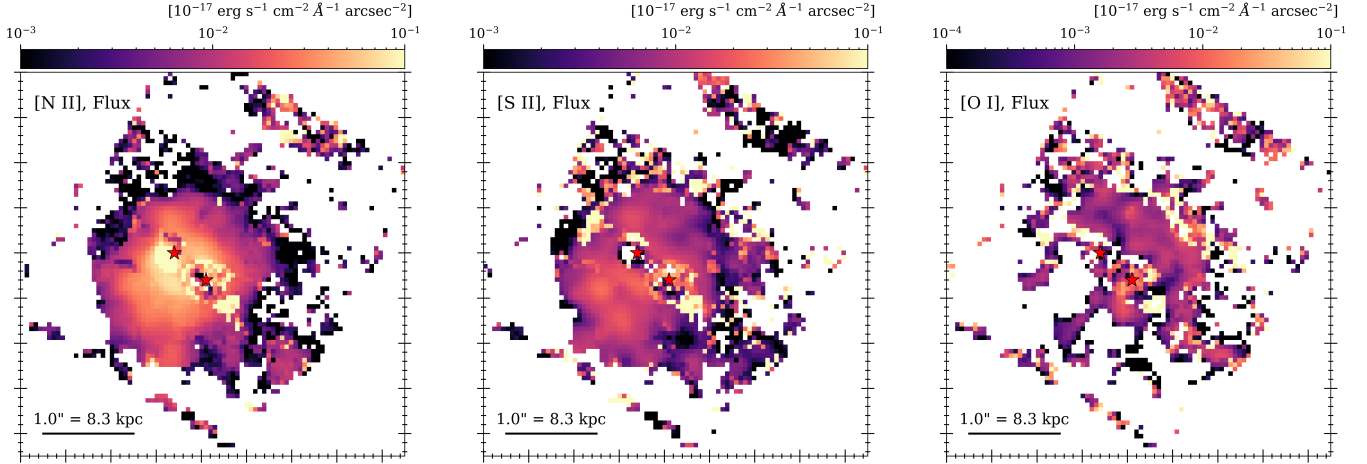


**Figure 5.** Intensity maps of [N II] (left), [S II] (center), and [O I] (right) produced with `q3dfit`. These lines are kinematically tied to  $H\alpha$ . We see that [N II] is more centrally concentrated, whereas [S II] and [O I] have uneven distributions around the quasars compared to  $H\alpha$  in Figure 4.

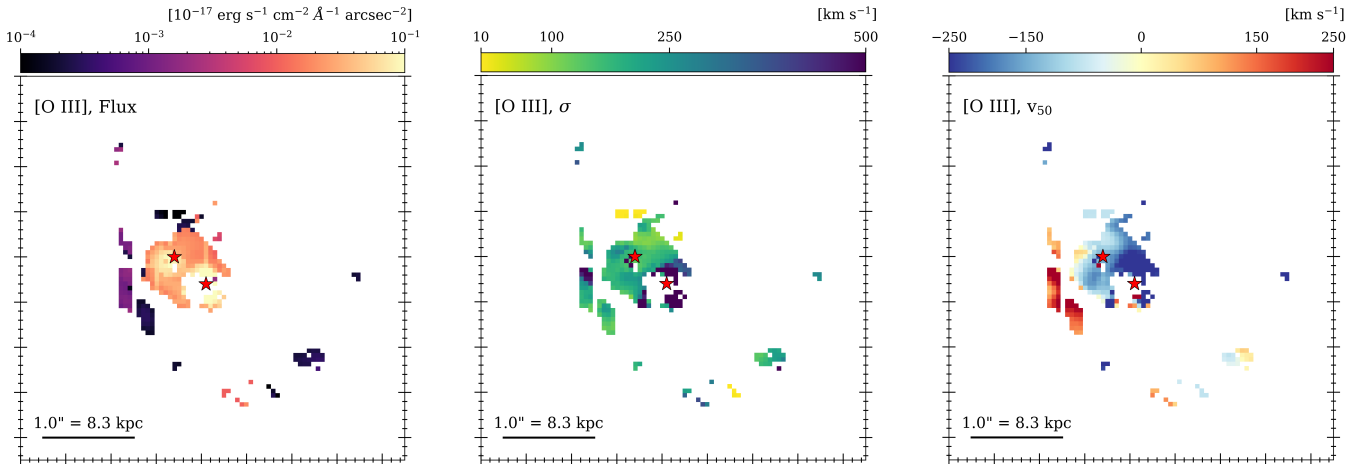


**Figure 6.** Intensity (left), velocity dispersion (center), and velocity (right) maps of the quasar-subtracted, narrow-line [O III] produced with `q3dfit`. Compared to the  $H\alpha$  maps, we see that [O III] has a much smaller spatial extent.

rotation field, whereas in a merger we expect each quasar to occupy either the red- or blue-shifted sides.

In addition to the narrow  $H\alpha$  emission, we also detect faint extended narrow line  $H\beta$ , [O III], [O I], [N II], and [S II], although they are not as luminous or extended as  $H\alpha$ . We also detect high-ionization lines such as [Ne V]  $\lambda\lambda 3426, 3729\text{\AA}$ . We show the intensity maps of the narrow [N II], [S II] and [O I] in Figure 5. In Figure 6 we show the intensity and kinematic maps of [O III]. Both [N II] and [S II] are co-spatial with the extended  $H\alpha$  that surround the two quasars. The [O I] emission is mostly concentrated in the northwest. In contrast,  $H\beta$  and [O III] emission is more compact and clumpy, mostly centered around J0749-NE, as seen in Figure 6. Interestingly, [O III] is fainter around J0749-SW, despite

it being the more luminous of the two quasars. The velocity structure of [O III] is also slightly different from that of  $H\alpha$  with a greater number of blueshifted clumps dominating the regions between J0749-NE and J0749-SW. Although there are regions with large [O III] velocity offsets reaching  $\Delta v \sim 400 \text{ km s}^{-1}$ , the associated velocity dispersion is small, so it is unlikely that J0749 has any large-scale outflows such as those found in recent JWST observations of luminous quasars at cosmic noon (e.g., Wylezalek et al. 2022; Vayner et al. 2023a; Veilleux et al. 2023).

### 3.2.3. Host-galaxy Ionization

We use optical line diagnostics (Baldwin et al. 1981; Veilleux & Osterbrock 1987) to investigate the ioniza-

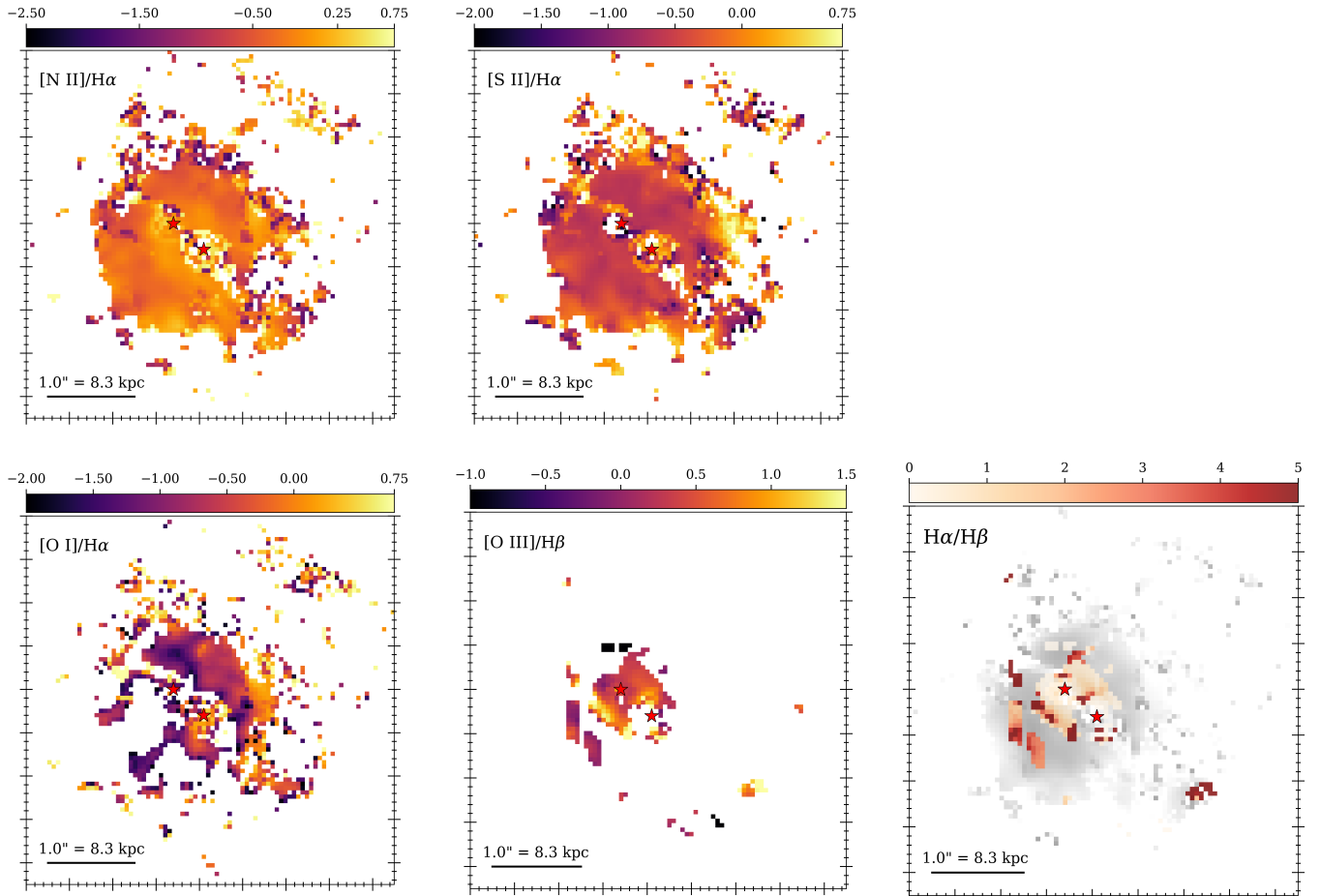


**Figure 7.** We show the  $[\text{N II}]/\text{H}\alpha$  (top left),  $[\text{S II}]/\text{H}\alpha$  (top right),  $[\text{O I}]/\text{H}\alpha$  (bottom left),  $[\text{O III}]/\text{H}\beta$  (bottom center), and  $\text{H}\alpha/\text{H}\beta$  (bottom right) line ratio plots. The  $\text{H}\alpha/\text{H}\beta$  line ratio map is overplotted over the extended  $\text{H}\alpha$  map shown in gray. The  $[\text{O III}]$  and  $\text{H}\beta$  emissions are much more centrally concentrated, which prevents us from a complete BPT/VO87 diagnostic shown in Figure 8.

tion mechanisms of the observed line emission, hereafter BPT (Baldwin et al. 1981) and VO87 (Veilleux & Osterbrock 1987). We take the emission line maps and measure the  $[\text{N II}]/\text{H}\alpha$ ,  $[\text{S II}]/\text{H}\alpha$ ,  $[\text{O I}]/\text{H}\alpha$ , and  $[\text{O III}]/\text{H}\beta$  line ratios. Measuring the  $[\text{O III}]/\text{H}\beta$  ratio is difficult at large scales because the  $\text{H}\beta$  and  $[\text{O III}]$  emission lines are faint and not as extended as the  $\text{H}\alpha$  system. We show the line ratio maps in Figure 7.

We show the BPT ( $[\text{N II}]/\text{H}\alpha$  vs.  $[\text{O III}]/\text{H}\beta$ ) and VO87 ( $[\text{S II}]/\text{H}\alpha$  vs.  $[\text{O III}]/\text{H}\beta$  and  $[\text{O I}]/\text{H}\alpha$  vs.  $[\text{O III}]/\text{H}\beta$ ) measurements along with the theoretical lines delineating photoionization by star formation, quasar, and shocks in Figure 8. Studies show that at higher redshifts, the effects of harder ionization spectra, lower gas and stellar metallicities, and denser interstellar medium push the separation between the star-formation and active galactic nuclei (AGN) or quasar ionization above the classic  $z = 0$  line (Kauffmann et al. 2003) in

the BPT diagram. We adopt the Kewley et al. (2013) formalism to calculate star formation in J0749. Using the Kewley et al. (2013) criteria at  $z = 2.17$ , we map the associated star for ionization regions in Figure 8. We also plot the BPT and VO87 diagrams and map the associated ionization regions. We can see that the gas in J0749 is a mix of quasar photoionization (in purple) and star-formation (in yellow) with some shock ionization (in green) hinted from elevated  $[\text{O I}]$  emission close to the quasars. The extended regions are mostly dominated by star formation. Although ionization at large distances from the quasar is likely due to star formation, it is difficult to determine the ionization mechanisms in these regions. They are likely dominated by star formation due to the faint nature of  $\text{H}\beta$  and  $[\text{O III}]$  at these distances. The large star-forming clumps to the south-east of the quasars show high  $\text{H}\alpha/\text{H}\beta$  suggesting dusty star formation.

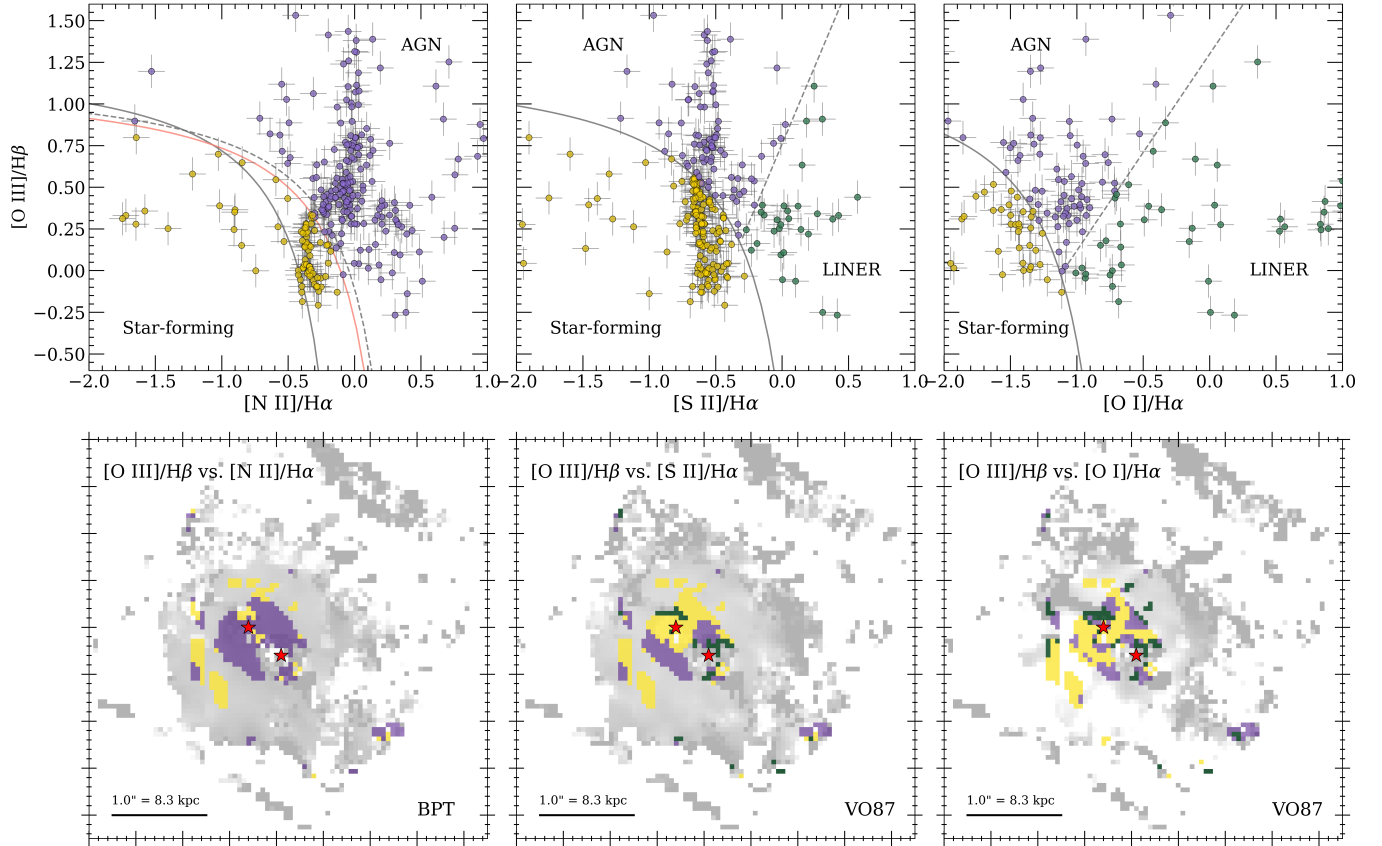


**Figure 8.** We show the spatially-resolved  $[O\ III]/H\beta$  vs.  $[N\ II]/H\alpha$  BPT (top left),  $[O\ III]/H\beta$  vs.  $[S\ II]/H\alpha$  VO87 (top center), and  $[O\ I]/H\alpha$  vs.  $[S\ II]/H\alpha$  VO87 (top right) ionization diagrams. We show the line that separates star formation and AGN/quasar photoionization. The BPT diagram (top left) shows the solid gray line ( $z = 0$  model; Kauffmann et al. 2003), dashed gray line (maximal  $z = 3$  model; Kewley et al. 2001), and solid red line ( $z = 2.17$  model; Kewley et al. 2013). The VO87 diagrams (top center and top right) shows the solid gray line separating star formation and AGN photoionization, and a dashed line separating quasar and LINER-like shock ionization. The points on the BPT and VO87 diagrams are color-coded to match the corresponding spatial positions shown in the bottom row: (bottom left) BPT map and (bottom center and right) VO87 map. The gray regions mark the  $[N\ II]/H\alpha$ ,  $[S\ II]/H\alpha$ , and  $[O\ I]/H\alpha$  fluxes from Figure 7 overlaid with quasar photoionized (purple), star-forming (yellow), and shock ionized (green) regions.

Considering the high luminosities of the two quasars ( $L_{bol} \sim 10^{46}$  erg  $s^{-1}$ ; Table 1), it is not surprising to find the inner regions to be dominated by quasar photoionization. It is more intriguing to find streams of star-forming regions centered on J0749-NE. There are some indications of star-forming streams connecting the two quasars towards the northwest (blueshifted  $H\alpha$ ). The star-forming streams are best traced by the  $[S\ II]/H\alpha$  and  $[O\ I]/H\alpha$  line ratio diagnostics, shown in Figure 8. The extended  $[N\ II]$  and  $[S\ II]$  emission also show low  $[N\ II]/H\alpha$  and  $[S\ II]/H\alpha$ , although the  $H\beta$  and  $[O\ III]$  are not detected. Since there is no evidence for widespread quasar-driven outflows, the likely explanation for the extended  $H\alpha$ ,  $[N\ II]$ , and  $[S\ II]$  is ionization due to low levels of star formation; the  $H\alpha$  surface brightness in these regions are nearly  $\times 10$  fainter than the central regions.

The total  $H\alpha$  flux associated with these star-forming regions is  $6.0 \times 10^{-15}$  erg  $s^{-1}$   $cm^{-2}$ , which translates to a star formation rate (SFR) of  $1,700 M_{\odot} \text{ yr}^{-1}$  based on the empirically derived conversion between  $H\alpha$  luminosity and SFR (Kennicutt 1998). If we account for additional contribution from quasar photoionization in the central regions this SFR estimate may be an upper limit, but it is clear that the SFR is very high. Assuming a stellar mass of  $10^{11.78} M_{\odot}$  (Chen et al. 2023), we obtain a specific SFR of  $2.7 \text{ Gyr}^{-1}$ . The results are qualitatively in agreement with the recent finding by Chen et al. (2024) based on the *JWST*/MIR data that the host galaxy of J0749 is undergoing very active star-formation.

In addition to the star-forming streams, the elevated  $[S\ II]/H\alpha$  and  $[O\ I]/H\alpha$  line ratios suggest small re-

regions of shock ionization. These shock regions are concentrated in the central regions along the star-forming streams and the quasar ionization. This may suggest shock heating. These regions also show elevated velocity dispersion reaching  $\sigma \sim 150 \text{ km s}^{-1}$  but show modest velocity offsets of  $\sim 100 \text{ km s}^{-1}$ . The likely culprits of the observed shock signatures are ionization from star-formation (or stellar feedback) in the dense interstellar medium, tidal shocks due to a merger (Rich et al. 2015), or quasar-driven outflows. However, there is no evidence for outflows in the line kinematics. The detection of extended high-ionization [Ne v] lines (require 97.11-126.21 eV) necessitates the presence of extreme photoionizing sources, such as a quasar, extreme ionizing stars (e.g. Wolf-Rayet), or supernova shocks (Cléri et al. 2023, and references therein). Given the complex environment of J0749 we may see a mix of ionizing sources.

We also map the  $H\alpha/H\beta$  line ratio to estimate the Balmer decrement. The Balmer decrement of the broad  $H\alpha$  and  $H\beta$  lines indicate little reddening or obscuration close to the quasar. However, the narrow line ratio around the quasars, especially around J0749-SW is higher, suggesting extinction at larger, galactic scales. Assuming the  $R_V = 3.1$  dust extinction model (Cardelli et al. 1989), we obtain a range of extinction up to  $A_V \approx 1.75$  mag, greatest around J0749-SW. In Section 3 we noted that the J0749-NE quasar has a slightly redder continuum than that of J0749-SW, which is in contrast to the line/gas-reddening. This may suggest that galactic reddening on top of the differences in the quasar continuum slopes (Chen et al. 2023) may be at play.

#### 4. DISCUSSION AND SUMMARY

To date, *JWST*/NIRSpec IFU has been extremely successful at revealing the complex gas structures of quasar host galaxies (e.g., Wylezalek et al. 2022) at cosmic noon. This is one of the first *JWST* study of a close-separation dual quasar in the early universe. Here, we discuss the properties of the two black holes and their host galaxies as revealed by *JWST*.

##### 4.1. Dual quasar or lensed quasar?

Distinguishing between lensed quasars and dual quasars is difficult. Chen et al. (2023) ruled out gravitational lensing in J0749 based on the non-detection of a foreground lens source, indirect detection of tidal tails from the host galaxy, and detection of X-ray and radio emission with chromatic differences. However, the new *JWST* observations of the two quasars revealed two surprisingly similar spectra, which required another look at the lensing hypothesis. In Figure 2 we show the multi-wavelength observations (SDSS, HST, and Gem-

ini) previously obtained by Chen et al. (2023) and with *JWST*/NIRSpec.

As outlined in Section 3, a close inspection of the two quasar spectra reveals subtle, yet clear differences in the continuum shape, emission line profiles (e.g.  $H\beta$ , [O III],  $H\alpha$ , He I), and even the Fe II emission features. We see a clear divergence in the quasar continuum redward of  $H\alpha$  as shown in the flux ratio in Figure 2, which is consistent with the differences in the rest-frame UV continuum slope measured by Chen et al. (2022). The best-fit emission line profiles determined with PyQSOFit suggest clear differences in the line shapes: J0749-NE has a smaller broad line component and stronger narrow line emission compared to those of J0749-SW, resulting in “pointier” spectral profiles as shown in Figure 3. Although one may argue that a lensed quasar with time delays can explain the differences in the observed emission line profiles, we also measure velocity offsets between the two quasars of up to  $\Delta v \sim 200 \text{ km s}^{-1}$ , which is inconsistent with the lensed quasar scenario.

In addition to the subtle spectral differences of the two quasars, *JWST*/NIRSpec detects the faint, extended host galaxy traced by multiple narrow emission lines (e.g. [O III],  $H\alpha$ ,  $H\beta$ ) at the same redshift as the two quasars. The narrow  $H\alpha$  emission line regions extend nearly  $2''$  or 16 kpc in diameter. Moreover, the extended emission corresponding to each narrow line shows different distributions. Kinematic analysis of the extended narrow  $H\alpha$  suggests a large rotating disk, whereas the [O III] emission is concentrated in between the quasars, and the [O I] emission is concentrated in the northwestern regions of the quasars (see Figures 4, 5, and 6). If J0749 is indeed lensed with two quasar+host galaxy images, then we would expect two identical spectra, which is inconsistent with observations. Also, we would expect the quasar+host galaxy images to appear flipped, including the kinematics, based on the lensing image parity relative to the lensing source. Instead, we see one normal-looking rotating disk with a symmetric red/blueshifted kinematic map.

There are alternative scenarios in which a foreground lens may produce two quasar+host images, but we did not find any indication of a foreground lens – either through imaging or spectroscopy. The morphology of the extended emission does not resemble arcs caused by lensing, and the observed appearance of the two quasars is inconsistent with expectations from a lensing model Chen et al. (2023). The spectral differences also argue against a scenario with a quasar and scattered light off nearby clouds producing two similar images. Furthermore, there is no evidence of absorption lines features Mg II and Fe II doublet/triplets by a putative lens

galaxy, such as those discovered by Gross et al. (2023). Differential magnification or even differential reddening by a foreground lens galaxy may alter the continuum shape and line intensities and produce spectrally different appearances (e.g., Agnello et al. 2018). Although exotic and unlikely lensing possibilities such as an extremely faint, massive lens (e.g. an ultra-diffuse galaxy) cannot be ruled out completely, the current evidence disfavors a lens scenario.

Thus, the only compelling, yet non-negligible, argument in favor of a lensed quasar is the observation of two quasars with similar spectra. If J0749 is indeed a physical pair, then their quasar spectra may be indicative of interesting accretion physics, perhaps unique to dual quasars.

#### 4.2. Enhanced quasar accretion

In summary, our latest *JWST*/NIRSpec IFU observations strongly suggest that J0749 is a real physically separated dual quasar with similar  $M_{\text{BH}}$ . The mystery of why the two quasars appear similar remains. Although we see the continuum of both quasars is consistent with rest-frame observations with SDSS, HST/STIS, and Gemini/GMOS, we see that there is a considerable difference in the rest-frame infrared with Gemini/GNIRS. This highlights the difficulty of resolving close-separation quasars using ground-based observatories in the infrared, pointing to the importance of the infrared sensitivity and resolving power of *JWST*. Our results are summarized in Table 1.

A notable feature uncovered by *JWST* is the strong rest-frame optical Fe II emission. Eigenvectors of quasars are believed to trace various fundamental parameters of quasar accretion such as mass accretion, covering factor of the Broad Line Region (BLR) clouds, the geometry of accretion, kinematics, ionization, and anisotropy of emitted radiation (Boroson & Green 1992). The group with strong optical Fe II, weak [O III], and high  $L/L_{\text{Edd}}$  are along one end of the Eigenvector 1 (or EV1) quasars. Although the EV1 properties have been defined for  $z < 1$  targets, there are very few studies of EV1s quasars at cosmic noon (Deconto-Machado et al. 2023). J0749 is consistent with EV1 quasars as seen in Figure 3.

The origin of Fe II emission is debated: either Fe II arises at or close to the BLR (Boroson & Green 1992) or outside of the BLR (Hu et al. 2008). The broad Fe II FWHM ( $\sim 5000 \text{ km s}^{-1}$ ) detected in J0749 may suggest that the observed Fe II originate at or close to the BLR of the respective SMBH. Based on  $M_{\text{BH}}$  values calculated using  $\text{H}\alpha$  and  $\text{H}\beta$ , both quasars have large  $\lambda_{\text{Edd}}$ , possibly due to enhanced inflows caused by the

merger or dynamical interactions. Thus, both quasars in J0749 are consistent with being high  $\lambda_{\text{Edd}}$  quasars like EV1 quasars. This is consistent with the model that EV1 quasars lie at the high end of the  $\lambda_{\text{Edd}}$  distribution (Boroson 2002; Shen & Ho 2014). Being both at one end of the EV1 sequence with high Eddington ratios, it is somewhat expected to have similar spectra for both quasars.

Another interpretation of EV1 quasars with strong Fe II and weak [O III] is that they are wind-dominated (e.g. Boroson & Green 1992; Marziani et al. 2018). Yet, there is no evidence for nuclear- or NLR-scale winds in J0749. In the UV/optical/IR spectrum, C IV seems to be at the same systemic redshift with no blueshift. This may indicate that quasar feedback, in the form of outflows, in J0749 is not (yet) a contributing factor in the dual quasar evolution.

Interestingly, there is no evidence of obscured accretion in the two quasars. The nuclear  $\text{H}\alpha/\text{H}\beta$  Balmer decrement is consistent with little dust reddening. X-ray observations reveal a Compton-thin environment (Chen et al. 2023). Theoretical predictions suggest that dual quasars would be heavily obscured at close separations (Blecha et al. 2018). Perhaps the separation between the J0749 quasars is too large such that accretion is not yet reaching extreme levels. In local Ultraluminous Infrared Galaxies (ULIRGs), the extinction peaks in the sub-kpc separations like Arp220 (Veilleux et al. 2009a). Another possibility is that the *Gaia* varstrometry selection is only sensitive to the non-dusty phase of quasar evolution (Hopkins et al. 2006). If true, then there may be a large population of obscured dual quasars waiting to be discovered, as suggested by Koss et al. (2018) and Barrows et al. (2023).

#### 4.3. Merger or massive disk galaxy?

The two quasars in J0749 are separated by 3.8 kpc and have similar black hole properties. With *JWST* we are for the first time able to detect the host galaxy gas in J0749 traced by the extended narrow emission lines (e.g.  $\text{H}\alpha$ ,  $\text{H}\beta$ , [O III]). Perhaps the most puzzling observation of J0749 is that we see two distinct quasars in what appears to be a large rotating gas disk that is best traced with the narrow  $\text{H}\alpha$   $v_{50}$  map in Figure 4. There are a few possible scenarios to understand J0749. Either we are observing an ongoing major galaxy merger with two active quasars or a large, single-disk galaxy hosting two active quasars.

The most natural scenario to form J0749 is through a major merger of gas-rich galaxies. There is some evidence that supports the merger scenario. Previously, Chen et al. (2023) used *HST*/F160W imaging to model

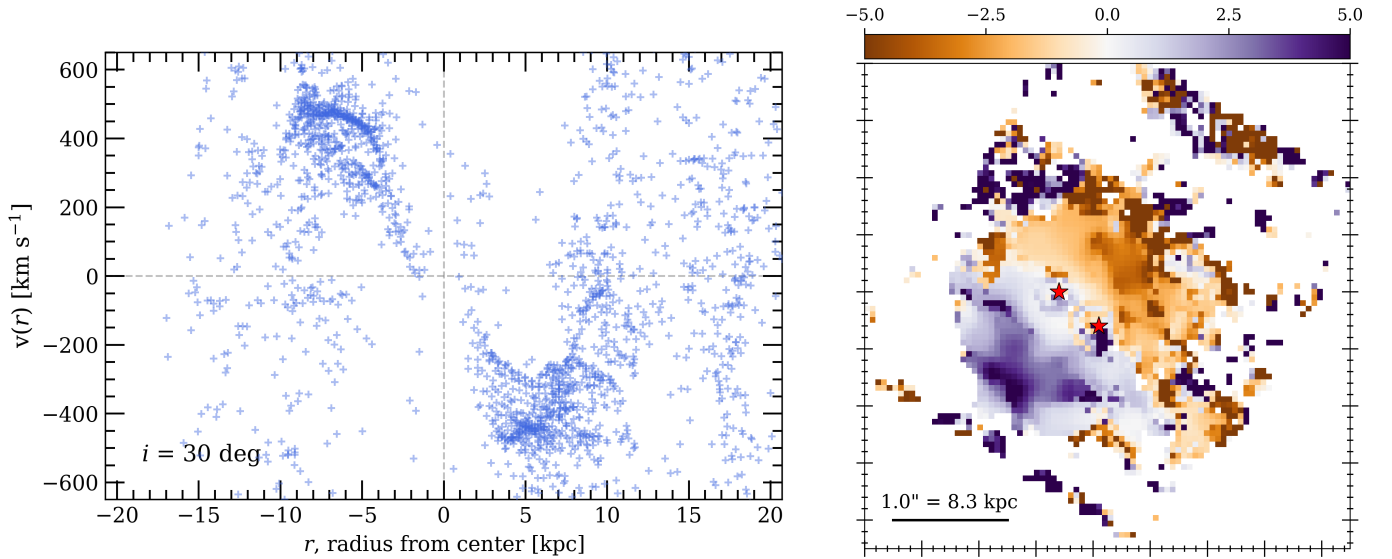


**Figure 9.** (Left) The deprojected  $v(r)$   $H\alpha$  rotation assuming an inclination angle of  $i = 30^\circ$  reveals a distinct rotation curve out to 10 kpc. There appears to be increased scatter beyond 10 kpc. (Right) The  $H\alpha$   $v/\sigma$ -ratio.

J0749 with two quasar PSFs and two Sersic host galaxies; this analysis shows an indirect detection of extended tidal tails. We confirm some of the *HST*/F160W features (T3 and T4 in Chen et al. 2023) that are located close to the two quasars with the NIRSspec detection of  $H\beta$  and  $[O\ III]$  as shown in Figure 6. Unfortunately, the JWST field-of-view is too small to confirm the most extended tails to the southwest and south. The bright spots on the southwest edge of the NIRSspec detector may be a detection of the T1 feature; however, we cannot rule out noise enhanced along the detector edges. Simulations also suggest the formation of gas disks following a major gas-rich merger (Barnes 2002), so we cannot rule out the merger-scenario.

Can the system “hide” a merger? Although kinematic maps can be used to distinguish between mergers and disks to some extent (Wisnioski et al. 2015), there are both observational and theoretical works that argue the opposite (Simons et al. 2019; Nevin et al. 2021). The conventional definition is that a rotating disk galaxy should exhibit a symmetric red-/blue-shifted  $v_{50}$  velocity map, while a merger would have a more asymmetric and highly disturbed velocity map (Wisnioski et al. 2015). However, Simons et al. (2019) showed that the merger-disk classification of  $z \sim 2$  galaxies using kinematic maps is not clear-cut since mergers can be disguised as disk galaxies, especially in the absence of sufficient signal-to-noise and spatial resolution. Nevin et al. (2021) also showed that the simulated kinematic selection of early-stage galaxy mergers can be unreliable since the stellar kinematics are still disk-like. One way

to break this degeneracy may be to compare the morphological and kinematic (mis)-alignments between the stellar and ionized gas components (Barrera-Ballesteros et al. 2015) in the future analysis of the stellar continuum data.

If J0749 is not a galaxy merger, then the alternative scenario is that J0749 is a massive galaxy hosting two massive black holes. Assuming that the host is indeed a massive rotating disk, we take the  $H\alpha$  kinematic maps and reconstruct the rotation curve of the host galaxy shown in Figure 9. The apparent major-minor axis ratio is  $\sim 1$ . This suggests a large disk appearing nearly face-on to us. If the elongation is based on the viewing inclination angle, then the host galaxy would at most have an inclination angle of  $i \approx 45^\circ$ , in which  $i \approx 90^\circ$  denotes the edge-on view of the galaxy. We take  $v_{50} = v(r) \cos \phi \sin i$  and calculate the rotation curve  $v(r, i)$  at increments  $i = 15^\circ, 30^\circ, \text{ and } 45^\circ$ . We plot  $v(r, i = 30^\circ)$  in Figure 9. From this, we calculate the dynamical mass of the massive disk galaxy  $M_{dyn} \sim 10^{12} M_\odot$  at  $r = 10$  kpc. The resultant  $M_{dyn}$  is much higher than that of star-forming galaxies at this epoch (Erb et al. 2006; Maseda et al. 2013), which may be an argument for the merger scenario. We also plot the  $v_{rot}/\sigma$  ratio, which does not show clear indication of turbulence according to Wisnioski et al. (2015).

Interestingly, simulations of  $z \sim 8$  and  $z < 1$  both predict the possibility of dual quasars hosted by a single galaxy (Rosas-Guevara et al. 2019; Mayer et al. 2023). In the Mayer et al. (2023) simulation, a major merger of two massive galaxies at  $z \sim 8$  is predicted to form a

nuclear supermassive disk. The instabilities of the disk (e.g. fast-rotating bars) can drive rapid gas inflows to the disk centers and may cause the gas to directly form a pair of massive black holes in the range  $10^6$  to  $10^8 M_\odot$  in the same galaxy. In this scenario, the two black holes feed from the same galactic gas reservoir, so it is plausible to have two active quasars with similar spectral accretion properties, effectively appearing like “twins.” Simulations by Rosas-Guevara et al. (2019) starts with a major galaxy merger and predicts that nearly 30% of simulated dual quasars may reside in a single host galaxy at  $z \sim 0.8-1$ . A caveat of these simulations is that they are both predicated on the assumption that a major galaxy merger precedes the formation of the black hole pairs.

Thus, simulations of 2 very different pathways show that it is possible for a single host galaxy to host two active quasars even at cosmic noon. If J0749 is indeed hosted by a massive disk, then this may call into question the conventional idea that a major merger leads to the formation of a dual quasar. Considering the inspiral time due to dynamical friction is  $t_{fric} \sim 0.22$  Gyr (Chen et al. 2023), it is unlikely for the dual quasar in J0749 to have formed at  $z > 3$  as in the Mayer et al. (2023) simulation. While a merger is the most plausible scenario, it is currently difficult to determine the exact formation history of J0749.

#### 4.4. Synchronized black hole accretion?

Whether or not J0749 resides in an ongoing merger, it is peculiar to find the two quasars with similar SMBH properties. Both are massive, reaching  $M_{BH} \sim 10^9 M_\odot$ . Selection effects by varstrometry are certainly involved (see Section 4.5). However, it is still important to explore the possible production pathways that would result in a dual quasar system like J0749.

Although empirical evidence connecting galaxy merger-driven gas inflows and quasar activity remains highly debated (e.g. Urrutia et al. 2008; Ellison et al. 2011; Glikman et al. 2015; Mechtley et al. 2016; Villforth et al. 2017; Ellison et al. 2019; Marian et al. 2019; Pierce et al. 2023; Breiding et al. 2023), numerical simulations have inferred a strong physical connection between major mergers and quasar triggering (Hopkins & Hernquist 2009; Torrey et al. 2020). A major gas-rich galaxy merger with two similar-mass black holes could be fueled. High  $\lambda_{Edd}$  may be allowed, but the two quasars may be constrained to a narrow range of  $\lambda_{Edd}$  and look identical. The exact  $\lambda_{Edd}$  are difficult to predict in these models since quasar accretion occurs on small scales not probed by galaxy-wide calculations. One possibility is a merger between two galaxies with

very similar pre-merger properties, perhaps within the same merger tree. Another possibility is a merger between a gas-rich and a gas-poor galaxy. In this case, the merger dynamics cause the gas to funnel toward the two galaxy cores, triggering both quasars. Simulations of dual quasars also suggest correlated growth of the two black holes in the late stage of the merger, especially at  $< 10$  kpc (Van Wassenhove et al. 2012). Thus, a merger-driven black hole fueling scenario may explain the “twin” quasar phenomenon observed in J0749.

A consequence of a “twin-quasar” scenario with similar accretion properties is that dual, synchronized quasars may disguise themselves as a bright single quasar in unresolved observation. If J0749-like properties are expected for dual quasars at close-separations, then discovering and characterizing close-separation  $< 1''$  dual quasars will remain a challenging task.

#### 4.5. Constraints on dual quasar selection

Lastly, we comment on the varstrometry technique to select dual quasar candidates. Interestingly, J0749 is a system of two similar-looking quasars with flux differences of only a factor of 3. Selection effects may contribute to the kinds of dual quasars discovered. Hwang et al. (2020) selected *Gaia* sources brighter than  $G < 19$  Vega mag to measure intrinsic variability to within a few percent. The magnitude selection is determined by the brightness limit of *Gaia*. This means that varstrometry is more efficient at uncovering intrinsically luminous  $z > 2$  pairs due to decreased contamination by the host galaxy (e.g. offset AGNs) and decreased lensing probability (Hwang et al. 2020; Shen et al. 2021). Moreover, *Gaia*-based varstrometry may preferentially select quasar pair candidates with similar fluxes; if one quasar dominates or the two black hole masses are too different, then the light centroid would be centered on the bright source and varstrometry may not detect any strong astrometric noise. These varstrometry-selected pairs may be lensed quasars (Li et al. 2023; Gross et al. 2023) or physical dual quasars with equal fluxes or have symbiotic accretion (like J0749). Distinguishing lensed and physical pairs requires extensive multiwavelength follow-up studies (Gross et al. 2023), including spatially-resolved observations.

It appears that the intrinsic abundance of quasar pairs, both lensed and physical pairs, at cosmic noon is low (Shen et al. 2023b), it would be interesting to see how many more dual quasars are hidden in plain sight. Currently, there are disagreements on the abundance of dual quasars across cosmic time (e.g. Silverman et al. 2020; Tang et al. 2021; Shen et al. 2023b; Perna et al. 2023), when comparing observations with predic-



tions from hydrodynamical simulations (e.g. De Rosa et al. 2019; Volonteri et al. 2022). A major challenge is that the division between lensed quasars and physical pairs remains unknown (Shen et al. 2023b), especially in the sub-arcsec regime. Furthermore, the properties of the dual quasar population remain unknown. It is currently difficult to determine if the discovery of close-separation dual quasars with similar quasar properties like J0749 (e.g. via symbiotic accretion) is statistically significant or is simply a selection effect.

There have been other confirmed dual quasars that exhibit similar spectral properties. For example, Koss et al. (2023) discussed a  $z = 0.03474$  dual AGN (UGC 4211) at 230 pc separation with remarkably similar optical spectra that indicate similar SMBH masses and velocity offsets between the two quasars reaching  $\sim 150 \text{ km s}^{-1}$ . However, unlike UGC 4211, J0749 shows strong Fe II emission, moderate  $H\beta$  emission with standard Balmer decrement values, and a rather large  $\lambda_{Edd}$ .

On the other hand, studies by Silverman et al. (2020); Tang et al. (2021) suggest that dual quasars have diverse properties. There are even some intriguing cases of a dual 6-kpc separation dual quasar that is quadruply lensed (Lemon et al. 2022). Although these cases may only encompass a minority of the dual and lensed populations, these peculiar discoveries accentuate the complexity and importance of detailed follow-up studies. This highlights the necessity for deep, spatially resolved, IR follow-up observations to confirm the nature of these objects, such as this project.

## 5. CONCLUSION

In this paper, we present JWST NIRSpec IFU observations of J0749, a dual quasar at  $z = 2.17$  with a physical separation of 3.8 kpc. J0749 was identified using the *Gaia*-based astrometric selection technique - VODKA. With JWST, we report the first direct detection of the faint host galaxy surrounding the two quasars. We analyze the NIRSpec IFU observations with `q3dfit`, which fits the datacube with quasar, polynomial continuum, and emission line models to decompose the spectra into the quasar PSFs and host galaxy. Previous multiwavelength imaging and spectroscopic observations of J0749 (i.e. Gemini, HST, Chandra, VLBA) spatially resolved the two quasars (J0749-NE and J0749-SW) and noted a faint detection of tidal tails possibly originating from their respective host galaxies (Chen et al. 2023). With JWST, we confirm the dual quasar nature and detect the extended ionized gas emission of the host galaxy that is best traced with the narrow  $H\alpha$  emission lines.

We obtain the aperture spectra of each of the two quasars, J0749-SW and J0749-NE, and fit them with

`PyQSOFit`. We find that both quasars show similar spectral properties. J0749-SW and J0749-NE have similar emission line widths and continuum shapes. Both quasars also show prominent Fe II line complexes. Their bolometric luminosities reach more than  $10^{46} \text{ erg s}^{-1}$ . Their single-epoch black hole masses are  $\sim 10^9 M_\odot$  and have relatively large  $\lambda_{Edd}$ . Despite their similar spectral appearances, careful comparison of the quasars' spectra reveals subtle differences. Most notably, the two quasars show clear velocity offsets of  $\sim 200 \text{ km s}^{-1}$ . Measurements of the velocity offsets and detection of the host galaxy at the same redshift as the quasars both disfavor a lensed quasar scenario. The similarity of the quasars suggests synchronized accretion scenario in which the two black holes are fueled simultaneously, possibly by the host galaxy dynamics.

Using `q3dfit` we decompose the two quasar spectra from the faint gas emission corresponding to the host galaxy and simultaneously fit the emission lines and continuum. We obtain intensity, velocity offset, and velocity dispersion maps of  $H\alpha$ ,  $H\beta$ , [O III], [N II], [S II], and [O I]. The narrow line  $H\alpha$  emission extends nearly  $2.5''$  or  $\sim 20 \text{ kpc}$  in diameter. The  $H\beta$  and [O III] emission are more compact, mostly centered around J0749-NE. No quasar-driven outflows are detected; there are no large velocity offsets corresponding to the narrow [O III] emission.

We present the analysis of the ionization physics of the host galaxy gas based on the optical emission line diagnostics based on [N II]/ $H\alpha$ , [S II]/ $H\alpha$ , [O I]/ $H\alpha$ , and [O III]/ $H\beta$ . The line ratio diagnostics show a mix of quasar ionization near the two quasars and large star-forming regions. The total  $H\alpha$  flux associated with star formation is  $6.0 \times 10^{-15} \text{ erg s}^{-1} \text{ cm}^{-2}$ , which translates to a star formation rate of  $1,700 M_\odot \text{ yr}^{-1}$  based on the Kennicutt (1998) conversion. This extremely high star formation rate is also seen in MIR diagnostics (Chen et al. 2024).

Surprisingly, the ionized  $H\alpha$  gas kinematics reveal a large, disk-like rotation curve, rather than an asymmetric profile that would be expected from an ongoing merger. The  $v_{50}$  is mostly symmetric, and we obtain a rotation curve similar to that of our Galaxy. Assuming that the  $H\alpha$  gas traces a single galaxy, we calculate the  $M_{dyn}$  to  $\sim 10^{12} M_\odot$ . We explore possible scenarios to explain the nature of J0749. Either J0749 is an ongoing gas-rich merger or it is a single disk galaxy hosting two luminous quasars. Intriguingly, both scenarios are allowed by simulations. Unfortunately, we are currently unable to disentangle the two scenarios.

This study shows that varstrometry is effective in uncovering dual quasar candidates. The selection method-

ology of varstrometry may preferentially select quasar pair candidates with similar fluxes, leading to the discovery of sources like J0749 with similar black hole properties ( $M_{\text{BH}}$  and  $L_{\text{bol}}$ ). However, this also complicates the task of distinguishing gravitationally lensed images from physical pairs. Doing so requires extensive multiwavelength and spatially resolved observations of the quasars and their host galaxy(ies). Thus, this study highlights the power and utility of integral field spectroscopy using JWST to study the interiors of galaxies at cosmic noon.

1 This work is based on observations made with the  
2 NASA/ESA/CSA James Webb Space Telescope. The  
3 data were obtained from the Mikulski Archive for Space  
4 Telescopes at the Space Telescope Science Institute,  
5 which is operated by the Association of Universities for  
6 Research in Astronomy, Inc., under NASA contract NAS  
7 5-03127 for JWST. These observations are associated  
8 with program #02654.

9 Support for program #02654 was provided by NASA  
10 through a grant from the Space Telescope Science Insti-  
11 tute, which is operated by the Association of Universities  
12 for Research in Astronomy, Inc., under NASA contract  
13 NAS 5-03127.

14 This work is supported by the Heising-Simons Foun-  
15 dation and Research Corporation for Science Advance-  
16 ment, and NSF grant AST-2108162 (XL, YS, YCC,  
17 AG).

18 D.S.N.R. was supported under program #DD-ERS-  
19 1335 from the Space Telescope Science Institute under  
20 NASA contract NAS 5-03127.

21 Y.I. thanks D. Coe, A-C. Eilers, E. Glikman, T. Heck-  
22 man, S. Knabel, D. Neufeld, M. Onoue, J. Silverman, Y.  
23 C. Taak, and M. Yue for useful discussions.

*Facilities:* JWST (NIRSpec)

*Software:* `astropy` (Astropy Collaboration et al. 2022), `q3dfit` (Rupke et al. 2023), `PyQSOFit` (Guo et al. 2018)

## REFERENCES

- Agnello, A., Grillo, C., Jones, T., et al. 2018, *MNRAS*, 474, 3391, doi: [10.1093/mnras/stx2950](https://doi.org/10.1093/mnras/stx2950)
- Arzoumanian, Z., Baker, P. T., Brazier, A., et al. 2018, *ApJ*, 859, 47, doi: [10.3847/1538-4357/aabd3b](https://doi.org/10.3847/1538-4357/aabd3b)
- Astropy Collaboration, Price-Whelan, A. M., Lim, P. L., et al. 2022, *ApJ*, 935, 167, doi: [10.3847/1538-4357/ac7c74](https://doi.org/10.3847/1538-4357/ac7c74)
- Baker, J. G., Centrella, J., Choi, D.-I., et al. 2006, *ApJL*, 653, L93, doi: [10.1086/510448](https://doi.org/10.1086/510448)
- Baldwin, J. A., Phillips, M. M., & Terlevich, R. 1981, *PASP*, 93, 5, doi: [10.1086/130766](https://doi.org/10.1086/130766)
- Barnes, J. E. 2002, *MNRAS*, 333, 481, doi: [10.1046/j.1365-8711.2002.05335.x](https://doi.org/10.1046/j.1365-8711.2002.05335.x)
- Barnes, J. E., & Hernquist, L. 1992, *ARA&A*, 30, 705, doi: [10.1146/annurev.aa.30.090192.003421](https://doi.org/10.1146/annurev.aa.30.090192.003421)
- Barrera-Ballesteros, J. K., García-Lorenzo, B., Falcón-Barroso, J., et al. 2015, *A&A*, 582, A21, doi: [10.1051/0004-6361/201424935](https://doi.org/10.1051/0004-6361/201424935)
- Barrows, R. S., Comerford, J. M., Stern, D., & Assef, R. J. 2023, *ApJ*, 951, 92, doi: [10.3847/1538-4357/acd2d3](https://doi.org/10.3847/1538-4357/acd2d3)
- Begelman, M. C., Blandford, R. D., & Rees, M. J. 1980, *Nature*, 287, 307, doi: [10.1038/287307a0](https://doi.org/10.1038/287307a0)
- Blaes, O., Lee, M. H., & Socrates, A. 2002, *ApJ*, 578, 775, doi: [10.1086/342655](https://doi.org/10.1086/342655)
- Blecha, L., Snyder, G. F., Satyapal, S., & Ellison, S. L. 2018, *MNRAS*, 478, 3056, doi: [10.1093/mnras/sty1274](https://doi.org/10.1093/mnras/sty1274)
- Bohlin, R. C., Gordon, K. D., & Tremblay, P. E. 2014, *PASP*, 126, 711, doi: [10.1086/677655](https://doi.org/10.1086/677655)
- Bohlin, R. C., & Landolt, A. U. 2015, *AJ*, 149, 122, doi: [10.1088/0004-6256/149/4/122](https://doi.org/10.1088/0004-6256/149/4/122)
- Bohlin, R. C., & Lockwood, S. 2022, Update of the STIS CTE Correction Formula for Stellar Spectra, Instrument Science Report STIS 2022-7, 11 pages
- Böker, T., Arribas, S., Lützgendorf, N., et al. 2022, *A&A*, 661, A82, doi: [10.1051/0004-6361/202142589](https://doi.org/10.1051/0004-6361/202142589)
- Boroson, T. A. 2002, *ApJ*, 565, 78, doi: [10.1086/324486](https://doi.org/10.1086/324486)
- Boroson, T. A., & Green, R. F. 1992, *ApJS*, 80, 109, doi: [10.1086/191661](https://doi.org/10.1086/191661)

- Breiding, P., Chiaberge, M., Lambrides, E., et al. 2023, arXiv e-prints, arXiv:2305.11804, doi: [10.48550/arXiv.2305.11804](https://doi.org/10.48550/arXiv.2305.11804)
- Cardelli, J. A., Clayton, G. C., & Mathis, J. S. 1989, *ApJ*, 345, 245, doi: [10.1086/167900](https://doi.org/10.1086/167900)
- Chen, Y.-C., Hwang, H.-C., Shen, Y., et al. 2022, *ApJ*, 925, 162, doi: [10.3847/1538-4357/ac401b](https://doi.org/10.3847/1538-4357/ac401b)
- Chen, Y.-C., Liu, X., Foord, A., et al. 2023, *Nature*, 616, 45, doi: [10.1038/s41586-023-05766-6](https://doi.org/10.1038/s41586-023-05766-6)
- Chen, Y.-C., Ishikawa, Y., Zakamska, N. L., et al. 2024, arXiv e-prints, arXiv:2403.04002, doi: [10.48550/arXiv.2403.04002](https://doi.org/10.48550/arXiv.2403.04002)
- Cleri, N. J., Yang, G., Papovich, C., et al. 2023, *ApJ*, 948, 112, doi: [10.3847/1538-4357/acce16](https://doi.org/10.3847/1538-4357/acce16)
- Colpi, M., & Dotti, M. 2011, *Advanced Science Letters*, 4, 181, doi: [10.1166/asl.2011.1205](https://doi.org/10.1166/asl.2011.1205)
- Comerford, J. M., Pooley, D., Barrows, R. S., et al. 2015, *ApJ*, 806, 219, doi: [10.1088/0004-637X/806/2/219](https://doi.org/10.1088/0004-637X/806/2/219)
- De Rosa, A., Vignali, C., Bogdanović, T., et al. 2019, *New Astronomy Reviews*, 86, 101525, doi: [10.1016/j.newar.2020.101525](https://doi.org/10.1016/j.newar.2020.101525)
- Deconto-Machado, A., del Olmo Orozco, A., Marziani, P., Perea, J., & Stirpe, G. M. 2023, *A&A*, 669, A83, doi: [10.1051/0004-6361/202243801](https://doi.org/10.1051/0004-6361/202243801)
- Di Matteo, T., Springel, V., & Hernquist, L. 2005, *Nature*, 433, 604, doi: [10.1038/nature03335](https://doi.org/10.1038/nature03335)
- Dotti, M., Ruzskowski, M., Paredi, L., et al. 2009, *MNRAS*, 396, 1640, doi: [10.1111/j.1365-2966.2009.14840.x](https://doi.org/10.1111/j.1365-2966.2009.14840.x)
- Ellison, S. L., Patton, D. R., Mendel, J. T., & Scudder, J. M. 2011, *MNRAS*, 418, 2043, doi: [10.1111/j.1365-2966.2011.19624.x](https://doi.org/10.1111/j.1365-2966.2011.19624.x)
- Ellison, S. L., Viswanathan, A., Patton, D. R., et al. 2019, *MNRAS*, 487, 2491, doi: [10.1093/mnras/stz1431](https://doi.org/10.1093/mnras/stz1431)
- EPTA Collaboration, InPTA Collaboration, Antoniadis, J., et al. 2023, *A&A*, 678, A50, doi: [10.1051/0004-6361/202346844](https://doi.org/10.1051/0004-6361/202346844)
- Erb, D. K., Steidel, C. C., Shapley, A. E., et al. 2006, *ApJ*, 646, 107, doi: [10.1086/504891](https://doi.org/10.1086/504891)
- Fu, H., Yan, L., Myers, A. D., et al. 2012, *ApJ*, 745, 67, doi: [10.1088/0004-637X/745/1/67](https://doi.org/10.1088/0004-637X/745/1/67)
- Gaia Collaboration. 2016, *A&A*, 595, A1, doi: [10.1051/0004-6361/201629272](https://doi.org/10.1051/0004-6361/201629272)
- Gardner, J. P., Mather, J. C., Clampin, M., et al. 2006, *SSRv*, 123, 485, doi: [10.1007/s11214-006-8315-7](https://doi.org/10.1007/s11214-006-8315-7)
- Glikman, E., Simmons, B., Maily, M., et al. 2015, *ApJ*, 806, 218, doi: [10.1088/0004-637X/806/2/218](https://doi.org/10.1088/0004-637X/806/2/218)
- Gould, A., & Rix, H.-W. 2000, *ApJL*, 532, L29, doi: [10.1086/312562](https://doi.org/10.1086/312562)
- Goulding, A. D., Pardo, K., Greene, J. E., et al. 2019, *ApJL*, 879, L21, doi: [10.3847/2041-8213/ab2a14](https://doi.org/10.3847/2041-8213/ab2a14)
- Gross, A. C., Chen, Y.-C., Foord, A., et al. 2023, *ApJ*, 956, 117, doi: [10.3847/1538-4357/acf469](https://doi.org/10.3847/1538-4357/acf469)
- Guo, H., Shen, Y., & Wang, S. 2018, PyQSOFit: Python code to fit the spectrum of quasars, Astrophysics Source Code Library, record ascl:1809.008. <http://ascl.net/1809.008>
- Heckman, T. M., & Best, P. N. 2014, *ARA&A*, 52, 589, doi: [10.1146/annurev-astro-081913-035722](https://doi.org/10.1146/annurev-astro-081913-035722)
- Hopkins, P. F., & Hernquist, L. 2009, *ApJ*, 694, 599, doi: [10.1088/0004-637X/694/1/599](https://doi.org/10.1088/0004-637X/694/1/599)
- Hopkins, P. F., Hernquist, L., Cox, T. J., et al. 2006, *ApJS*, 163, 1, doi: [10.1086/499298](https://doi.org/10.1086/499298)
- Hu, C., Wang, J.-M., Ho, L. C., et al. 2008, *ApJ*, 687, 78, doi: [10.1086/591838](https://doi.org/10.1086/591838)
- Hwang, H.-C., Shen, Y., Zakamska, N., & Liu, X. 2020, *ApJ*, 888, 73, doi: [10.3847/1538-4357/ab5c1a](https://doi.org/10.3847/1538-4357/ab5c1a)
- Jakobsen, P., Ferruit, P., Alves de Oliveira, C., et al. 2022, *A&A*, 661, A80, doi: [10.1051/0004-6361/202142663](https://doi.org/10.1051/0004-6361/202142663)
- Kauffmann, G., Heckman, T. M., Tremonti, C., et al. 2003, *MNRAS*, 346, 1055, doi: [10.1111/j.1365-2966.2003.07154.x](https://doi.org/10.1111/j.1365-2966.2003.07154.x)
- Kennicutt, Robert C., J. 1998, *ARA&A*, 36, 189, doi: [10.1146/annurev.astro.36.1.189](https://doi.org/10.1146/annurev.astro.36.1.189)
- Kewley, L. J., Dopita, M. A., Sutherland, R. S., Heisler, C. A., & Trevena, J. 2001, *ApJ*, 556, 121, doi: [10.1086/321545](https://doi.org/10.1086/321545)
- Kewley, L. J., Maier, C., Yabe, K., et al. 2013, *ApJL*, 774, L10, doi: [10.1088/2041-8205/774/1/L10](https://doi.org/10.1088/2041-8205/774/1/L10)
- Kharb, P., Lal, D. V., & Merritt, D. 2017, *Nature Astronomy*, 1, 727, doi: [10.1038/s41550-017-0256-4](https://doi.org/10.1038/s41550-017-0256-4)
- Koss, M. J., Blecha, L., Bernhard, P., et al. 2018, *Nature*, 563, 214, doi: [10.1038/s41586-018-0652-7](https://doi.org/10.1038/s41586-018-0652-7)
- Koss, M. J., Treister, E., Kakkad, D., et al. 2023, *ApJL*, 942, L24, doi: [10.3847/2041-8213/aca8f0](https://doi.org/10.3847/2041-8213/aca8f0)
- Lemon, C., Millon, M., Sluse, D., et al. 2022, *A&A*, 657, A113, doi: [10.1051/0004-6361/202142138](https://doi.org/10.1051/0004-6361/202142138)
- Li, J., Liu, X., Shen, Y., et al. 2023, *ApJL*, 955, L16, doi: [10.3847/2041-8213/acf27a](https://doi.org/10.3847/2041-8213/acf27a)
- LIGO Scientific Collaboration, & Virgo Collaboration. 2016, *Physical Review Letters*, 116, 061102, doi: [10.1103/PhysRevLett.116.061102](https://doi.org/10.1103/PhysRevLett.116.061102)
- Liu, X., Guo, H., Shen, Y., Greene, J. E., & Strauss, M. A. 2018, *ApJ*, 862, 29, doi: [10.3847/1538-4357/aac9cb](https://doi.org/10.3847/1538-4357/aac9cb)
- Liu, X., Shen, Y., Bian, F., Loeb, A., & Tremaine, S. 2014, *ApJ*, 789, 140, doi: [10.1088/0004-637X/789/2/140](https://doi.org/10.1088/0004-637X/789/2/140)
- Liu, Y. 2015, *A&A*, 580, A133, doi: [10.1051/0004-6361/201526266](https://doi.org/10.1051/0004-6361/201526266)
- . 2016, *A&A*, 592, L4, doi: [10.1051/0004-6361/201628430](https://doi.org/10.1051/0004-6361/201628430)
- Marian, V., Jahnke, K., Mechtley, M., et al. 2019, *ApJ*, 882, 141, doi: [10.3847/1538-4357/ab385b](https://doi.org/10.3847/1538-4357/ab385b)

- Marziani, P., Dultzin, D., Sulentic, J. W., et al. 2018, *Frontiers in Astronomy and Space Sciences*, 5, 6, doi: [10.3389/fspas.2018.00006](https://doi.org/10.3389/fspas.2018.00006)
- Maseda, M. V., van der Wel, A., da Cunha, E., et al. 2013, *ApJL*, 778, L22, doi: [10.1088/2041-8205/778/1/L22](https://doi.org/10.1088/2041-8205/778/1/L22)
- Mayer, L., Capelo, P. R., Zwick, L., & Di Matteo, T. 2023, arXiv e-prints, arXiv:2304.02066, doi: [10.48550/arXiv.2304.02066](https://doi.org/10.48550/arXiv.2304.02066)
- McAlpine, S., Bower, R. G., Rosario, D. J., et al. 2018, *MNRAS*, 481, 3118, doi: [10.1093/mnras/sty2489](https://doi.org/10.1093/mnras/sty2489)
- Mechtley, M., Jahnke, K., Windhorst, R. A., et al. 2016, *ApJ*, 830, 156, doi: [10.3847/0004-637X/830/2/156](https://doi.org/10.3847/0004-637X/830/2/156)
- Milosavljević, M., & Merritt, D. 2001, *ApJ*, 563, 34, doi: [10.1086/323830](https://doi.org/10.1086/323830)
- Nevin, R., Blecha, L., Comerford, J., et al. 2021, *ApJ*, 912, 45, doi: [10.3847/1538-4357/abe2a9](https://doi.org/10.3847/1538-4357/abe2a9)
- Perna, M., Arribas, S., Marshall, M., et al. 2023, *A&A*, 679, A89, doi: [10.1051/0004-6361/202346649](https://doi.org/10.1051/0004-6361/202346649)
- Pierce, J. C. S., Tadhunter, C., Ramos Almeida, C., et al. 2023, *MNRAS*, 522, 1736, doi: [10.1093/mnras/stad455](https://doi.org/10.1093/mnras/stad455)
- Rich, J. A., Kewley, L. J., & Dopita, M. A. 2015, *ApJS*, 221, 28, doi: [10.1088/0067-0049/221/2/28](https://doi.org/10.1088/0067-0049/221/2/28)
- Richards, G. T., Strauss, M. A., Fan, X., et al. 2006, *AJ*, 131, 2766, doi: [10.1086/503559](https://doi.org/10.1086/503559)
- Rodriguez, C., Taylor, G. B., Zavala, R. T., et al. 2006, *ApJ*, 646, 49, doi: [10.1086/504825](https://doi.org/10.1086/504825)
- Rosas-Guevara, Y. M., Bower, R. G., McAlpine, S., Bonoli, S., & Tissera, P. B. 2019, *MNRAS*, 483, 2712, doi: [10.1093/mnras/sty3251](https://doi.org/10.1093/mnras/sty3251)
- Rupke, D., Wylezalek, D., Zakamska, N., et al. 2023, q3dfit: PSF decomposition and spectral analysis for JWST-IFU spectroscopy, Astrophysics Source Code Library, record ascl:2310.004. <http://ascl.net/2310.004>
- Sanders, D. B., & Mirabel, I. F. 1996, *ARA&A*, 34, 749, doi: [10.1146/annurev.astro.34.1.749](https://doi.org/10.1146/annurev.astro.34.1.749)
- Schlawin, E., Leisenring, J., Misselt, K., et al. 2020, *AJ*, 160, 231, doi: [10.3847/1538-3881/abb811](https://doi.org/10.3847/1538-3881/abb811)
- Schneider, D. P., Richards, G. T., Hall, P. B., et al. 2010, *AJ*, 139, 2360, doi: [10.1088/0004-6256/139/6/2360](https://doi.org/10.1088/0004-6256/139/6/2360)
- Sesar, B., Ivezić, Ž., Lupton, R. H., et al. 2007, *The Astronomical Journal*, 134, 2236, doi: [10.1086/521819](https://doi.org/10.1086/521819)
- Shen, Y., & Ho, L. C. 2014, *Nature*, 513, 210, doi: [10.1038/nature13712](https://doi.org/10.1038/nature13712)
- Shen, Y., Hwang, H.-C., Zakamska, N., & Liu, X. 2019a, *ApJL*, 885, L4, doi: [10.3847/2041-8213/ab4b54](https://doi.org/10.3847/2041-8213/ab4b54)
- Shen, Y., & Liu, X. 2012, *ApJ*, 753, 125, doi: [10.1088/0004-637X/753/2/125](https://doi.org/10.1088/0004-637X/753/2/125)
- Shen, Y., Liu, X., Greene, J. E., & Strauss, M. A. 2011, *ApJ*, 735, 48, doi: [10.1088/0004-637X/735/1/48](https://doi.org/10.1088/0004-637X/735/1/48)
- Shen, Y., McBride, C. K., White, M., et al. 2013, *ApJ*, 778, 98, doi: [10.1088/0004-637X/778/2/98](https://doi.org/10.1088/0004-637X/778/2/98)
- Shen, Y., Hall, P. B., Horne, K., et al. 2019b, *ApJS*, 241, 34, doi: [10.3847/1538-4365/ab074f](https://doi.org/10.3847/1538-4365/ab074f)
- Shen, Y., Chen, Y.-C., Hwang, H.-C., et al. 2021, *Nature Astronomy*, 5, 569, doi: [10.1038/s41550-021-01323-1](https://doi.org/10.1038/s41550-021-01323-1)
- Shen, Y., Grier, C. J., Horne, K., et al. 2023a, arXiv e-prints, arXiv:2305.01014, doi: [10.48550/arXiv.2305.01014](https://doi.org/10.48550/arXiv.2305.01014)
- Shen, Y., Hwang, H.-C., Oguri, M., et al. 2023b, *ApJ*, 943, 38, doi: [10.3847/1538-4357/aca662](https://doi.org/10.3847/1538-4357/aca662)
- Silverman, J. D., Tang, S., Lee, K.-G., et al. 2020, *ApJ*, 899, 154, doi: [10.3847/1538-4357/aba4a3](https://doi.org/10.3847/1538-4357/aba4a3)
- Simons, R. C., Kassin, S. A., Snyder, G. F., et al. 2019, *ApJ*, 874, 59, doi: [10.3847/1538-4357/ab07c9](https://doi.org/10.3847/1538-4357/ab07c9)
- Stemo, A., Comerford, J. M., Barrows, R. S., et al. 2021, *ApJ*, 923, 36, doi: [10.3847/1538-4357/ac0bbf](https://doi.org/10.3847/1538-4357/ac0bbf)
- Tang, S., Silverman, J. D., Ding, X., et al. 2021, *ApJ*, 922, 83, doi: [10.3847/1538-4357/ac1fff](https://doi.org/10.3847/1538-4357/ac1fff)
- Torrey, P., Hopkins, P. F., Faucher-Giguère, C.-A., et al. 2020, *MNRAS*, 497, 5292, doi: [10.1093/mnras/staa2222](https://doi.org/10.1093/mnras/staa2222)
- Urrutia, T., Lacy, M., & Becker, R. H. 2008, *ApJ*, 674, 80, doi: [10.1086/523959](https://doi.org/10.1086/523959)
- Van Wassenhove, S., Volonteri, M., Mayer, L., et al. 2012, *ApJL*, 748, L7, doi: [10.1088/2041-8205/748/1/L7](https://doi.org/10.1088/2041-8205/748/1/L7)
- Vayner, A., Zakamska, N. L., Ishikawa, Y., et al. 2023a, *ApJ*, 955, 92, doi: [10.3847/1538-4357/ace784](https://doi.org/10.3847/1538-4357/ace784)
- . 2023b, arXiv e-prints, arXiv:2307.13751, doi: [10.48550/arXiv.2307.13751](https://doi.org/10.48550/arXiv.2307.13751)
- Veilleux, S., & Osterbrock, D. E. 1987, *ApJS*, 63, 295, doi: [10.1086/191166](https://doi.org/10.1086/191166)
- Veilleux, S., Rupke, D. S. N., Kim, D. C., et al. 2009a, *ApJS*, 182, 628, doi: [10.1088/0067-0049/182/2/628](https://doi.org/10.1088/0067-0049/182/2/628)
- Veilleux, S., Kim, D. C., Rupke, D. S. N., et al. 2009b, *ApJ*, 701, 587, doi: [10.1088/0004-637X/701/1/587](https://doi.org/10.1088/0004-637X/701/1/587)
- Veilleux, S., Liu, W., Vayner, A., et al. 2023, *ApJ*, 953, 56, doi: [10.3847/1538-4357/ace10f](https://doi.org/10.3847/1538-4357/ace10f)
- Villforth, C., Hamilton, T., Pawlik, M. M., et al. 2017, *MNRAS*, 466, 812, doi: [10.1093/mnras/stw3037](https://doi.org/10.1093/mnras/stw3037)
- Volonteri, M., Bogdanović, T., Dotti, M., & Colpi, M. 2016, *IAU Focus Meeting*, 29B, 285, doi: [10.1017/S1743921316005366](https://doi.org/10.1017/S1743921316005366)
- Volonteri, M., Pfister, H., Beckmann, R., et al. 2022, *MNRAS*, 514, 640, doi: [10.1093/mnras/stac1217](https://doi.org/10.1093/mnras/stac1217)
- Wisnioski, E., Förster Schreiber, N. M., Wuyts, S., et al. 2015, *ApJ*, 799, 209, doi: [10.1088/0004-637X/799/2/209](https://doi.org/10.1088/0004-637X/799/2/209)
- Wylezalek, D., Vayner, A., Rupke, D. S. N., et al. 2022, *ApJL*, 940, L7, doi: [10.3847/2041-8213/ac98c3](https://doi.org/10.3847/2041-8213/ac98c3)
- Yu, Q. 2002, *MNRAS*, 331, 935, doi: [10.1046/j.1365-8711.2002.05242.x](https://doi.org/10.1046/j.1365-8711.2002.05242.x)

Zakamska, N. L., Lampayan, K., Petric, A., et al. 2016,  
*MNRAS*, 455, 4191, doi: [10.1093/mnras/stv2571](https://doi.org/10.1093/mnras/stv2571)